Chapter 2

Fundamentals

2.1 THEORY OF WATER FLOW AND HEAT TRANSPORT IN THE SUBSURFACE

The modeling of water flow and heat transport processes in the subsurface has to be based on a **mathematical formulation** of the various processes occurring in a considered spatial domain of the subsurface. Such a mathematical formulation provides a compact description of the relevant processes and includes initial and boundary conditions thus representing a model of the complex reality. Furthermore, it lists all assumptions and simplifications, which are postulated. The considered domain extends horizontally and vertically, the size depending on expected length scales of the processes, as well as on possibilities to formulate proper boundary conditions for the related variables like temperature or infiltration rate. For the modeling of heat transfer in shallow subsurface systems, **the considered domain typically includes the soil surface** where it is feasible to formulate thermal boundary conditions. This means, for the case of shallow unconfined groundwater systems, that, in general, the unsaturated zone (also referred to as capillary zone) has to be taken into account. Physical processes essentially comprise hydraulic and thermal processes in porous media. Heat generation by chemical or biochemical reactions or by radioactive decay is not assumed to be of importance in the case of heat transport in the subsurface. Thus, the relevant processes considered here comprise the flow of water and the heat transport in both the unsaturated and the saturated zones of the subsurface.

2.1.1 Modeling hydraulic processes in porous media

2.1.1.1 Flow in saturated and unsaturated porous media, Darcy's law

Hydraulic processes are important for heat transport whenever advective heat flux, by flowing water, is significant. Also in the case of stagnant or

static conditions, the water content plays a role in the thermal parameters. When considering hydraulic processes in connection with thermal propagation, we have to be aware that essential physical parameters of flow processes, like **water density** and **water viscosity**, are temperature dependent. In general, water density ρ_w (kg m^{-3}) and dynamic water viscosity μ_w (Pa s) are considered to be functions of water pressure p_w, concentration c of dissolved substances, and temperature T (°C), or $\rho_w = \rho_w (p_w, c, T)$ and $\mu_w = \mu_w (p_w, c, T)$. While temperature dependence of water density leads to density effects in flow problems (with maximum water density close to 4°C), the temperature dependence of water viscosity leads to decreasing viscosity values for increasing temperature (Figure 2.1). Typical values are shown in Section 2.2. The temperature

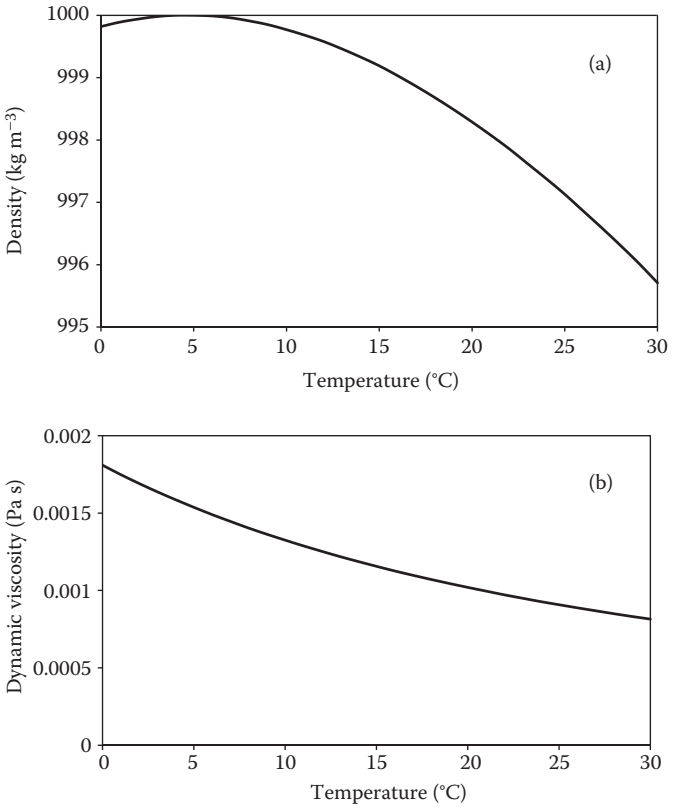

Figure 2.1 Temperature dependence of water density (a) and water viscosity (b). (Data from www.thermexcel.com.)

dependence of water viscosity directly affects **hydraulic conductivity** $\mathbf{K}_w$ (m s^{-1}) (Bear 1979), that is,

$$\mathbf{K}_w(T) = \frac{\mathbf{k} g \rho_w(p_w, c, T)}{\mu_w(p_w, c, T)} \tag{2.1}$$

where $\mathbf{k}$ (m^2) is the permeability tensor of the porous medium, which depends solely on the geometrical configuration of the porous matrix, and g is the acceleration due to gravity. This means that, for example, hydraulic conductivity at 20°C is about 1.5 times higher than at 5°C due to the change in water viscosity.

A consequence of the temperature dependence is that the **general form of Darcy's law** (Bear 1979) for expressing water fluxes should be used, that is,

$$\mathbf{q}_w = -\frac{\mathbf{k}}{\mu_w(p_w, c, T)}[\nabla p_w - \rho_w(p_w, c, T)\mathbf{g}] \tag{2.2}$$

where $\mathbf{q}_w$ (m s^{-1}) is the specific flux vector (Darcy velocity), ∇ is the gradient operator, p_w is the water pressure (Pa) and $\mathbf{g}$ (m s^{-2}) is the vector of acceleration due to gravity having the form $\mathbf{g} = (0, 0, -g)$, for a vertical z-axis pointing upward. Equation 2.2 can be written as balance of the **forces acting** per unit volume of water:

$$-\frac{\mathbf{q}_w \mu_w(p_w, c, T)}{\mathbf{k}} - \nabla p_w + \rho_w(p_w, c, T)\mathbf{g} = 0 \tag{2.3}$$

The first term denotes the **friction force**, the second one the **water pressure force**, and the third term is the **gravity force**, all per unit volume.

By introducing a **constant reference temperature** T_0 (e.g., mean temperature at soil surface) and a **constant reference pressure** $p_{w,0}$, and by restricting the analysis to **constant concentrations** $c = c_0$ in the following, the **water density** can be approximated by linear expansion as follows:

$$\begin{aligned}\rho_w(p_w, T) &\simeq \rho_w(p_{w,0}, T_0) + \left(\frac{\partial \rho_w}{\partial T}\right)_{T_0, p_{w,0}} (T - T_0) + \left(\frac{\partial \rho_w}{\partial p_w}\right)_{T_0, p_{w,0}} (p_w - p_{w,0}) \\ &\simeq \rho_{w,0}[1 + b_p(p_w - p_{w,0}) + b_T(T - T_0)]\end{aligned} \tag{2.4}$$

with $\rho_{w,0} = \rho_w(p_{w,0}, T_0)$. The coefficients b_p and b_T with

$$b_p = \frac{1}{\rho_{w,0}} \frac{\partial \rho_w}{\partial p_w}; \quad b_T = \frac{1}{\rho_{w,0}} \frac{\partial \rho_w}{\partial T} \tag{2.5}$$

are the compressibility and the thermal volume expansion coefficients for water. In an alternative formulation for ρ_w (p_w, T), the compressibility of water is neglected:

$$\rho_w(p_w,T) = \rho_w(p_w,T_0) + \Delta\rho_w(T, T_0) \simeq \rho_w(p_w, T_0)\,[1 + b_T\,(T - T_0)] \quad (2.6)$$

Based on Equation 2.6, Darcy's law (Equation 2.2) can be reformulated as follows:

$$\mathbf{q}_w = -\frac{\mathbf{k}}{\mu_w(p_w,T)}\left[\nabla p_w - \left(\rho_w(p_w,T_0) + \Delta\rho_w(T,T_0)\right)\mathbf{g}\right] \quad (2.7)$$

and the balance Equation 2.3 of acting forces is given by

$$-\frac{\mathbf{q}_w\mu_w\left(p_w,T\right)}{\mathbf{k}} - \nabla p_w + \rho_w(p_w,T_0)\mathbf{g} + \Delta\rho_w(T,T_0)\mathbf{g} = 0 \quad (2.8)$$

Based on this formulation, the effect of density variations due to temperature changes may be assessed. The ratio between the buoyancy force $\Delta\rho_w g$ acting vertically and the horizontal friction force from Darcy's law in a regional flow is in absolute values:

$$G = \frac{\Delta\rho_w}{\rho_{w,0}}\frac{k\mu_w}{q} = \frac{\Delta\rho_w}{\rho_{w,0}}\frac{K_w}{q} = \frac{\Delta\rho_w}{\rho_{w,0}I_{hor}} \quad (2.9)$$

The symbol I_{hor} is the horizontal flow gradient. Oostrom et al. (1992) called G a **stability number**, which they obtained from dimensional analysis. Based on experimental investigation, they determined a critical stability number of about G_c = 0.3. Woumeni and Vauclin (2006) confirmed the usefulness of the ratio in their field study on the coupled effects of aquifer stratification, fluid density, and groundwater fluctuations on dispersivity in solute transport. The stability number can be used to **assess the importance of density effects**. For **example**, if we inject water at a temperature of T = 9°C into an aquifer of initial temperature T_0 = 12°C, and with a horizontal flow gradient of I_{hor} = 0.001, the density difference $\Delta\rho_w$ is about 0.28 kg m^{-3}, and the ratio of Equation 2.9 is 0.28, thus only slightly smaller than the critical value. Even if density effects are present, due to mixing effects, these effects may gradually be reduced away from the injection point. Neglecting density effects may be acceptable at substantial temperature differences between injected water and groundwater. This was shown by Ma and Zheng (2010) based on their modeling study of the Hanford site (United States). They found that for thermal tracer experiments, model

errors due to ignoring density effects are insignificant for temperature differences as large as 15°C across the entire model domain. Ward et al. (2007) concluded from their theoretical and numerical analysis that the relevance of density effects in aquifer storage and recovery depends on the relative influences of density difference, hydraulic conductivity, pumping rates, injected radius, storage duration, and dispersivity, thus confirming the importance of the flow condition.

In the case of thermal use of shallow subsurface systems with restricted temperature changes, **water density and viscosity are often used as constants in thermohydraulic models**, and thus, temperature dependence is disregarded. As a consequence, water flow is not affected by heat transport, and both equations can be handled and solved in an uncoupled and sequential manner. Since **flow processes represent an important element in thermal processes**, they are briefly compiled here.

Hydraulic processes can take place in both the **saturated and unsaturated zones**. For convenience, both zones are treated here simultaneously. In unconfined aquifers, the upper limit of the groundwater zone consists of the water table. The level of the water table is usually defined as the location with atmospheric water pressure (zero relative water pressure). Consequently, the domain above the water table is the unsaturated zone (or capillary zone, Figure 2.2). In principle, the capillary zone is hydraulically unsaturated by the simultaneous presence of water and air in a control volume. However, part of the capillary zone close to the water table can still be hydraulically saturated (saturated or quasi-saturated capillary fringe; Figure 2.2). The corresponding related relative water pressure in the capillary zone is negative (suction).

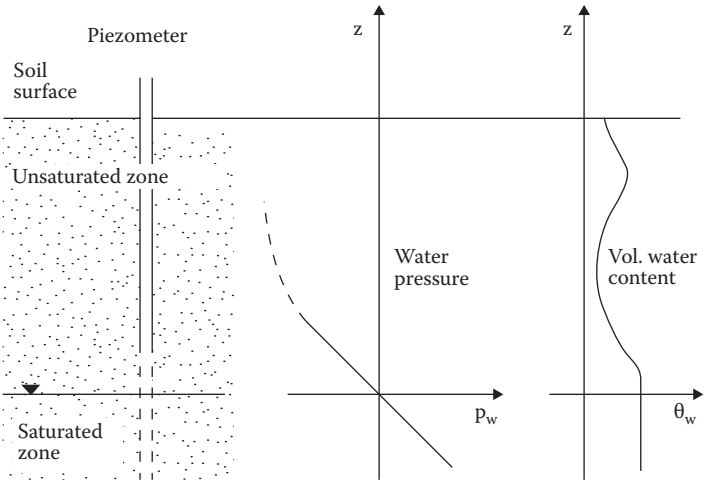

Figure 2.2 Capillary zone above a water table; vertical water pressure profile $p_w(z)$ and vertical profile of the volumetric water content $\theta_w(z)$ (schematic).

Flow in saturated porous media with constant water density is usually described by the following form of **Darcy's law**, which is directly based on Darcy's postulation:

$$\mathbf{q}_w = -\mathbf{K}_w \nabla h_w \tag{2.10}$$

where h_w (m) is the piezometric head (or head) with

$$h_w = z + \frac{p_w}{\rho_w g} \tag{2.11}$$

Darcy's law states that the flow rate is proportional to the head gradient. The variable z(m) is the vertical coordinate (positive upward). The equations can also be obtained from Equations 2.1 and 2.2 by setting the water density ρ_w to a constant.

Hydraulic conductivity $\mathbf{K}_w(\mathbf{x})$ at location $\mathbf{x}(x, y, z)$ (m) usually exhibits strong spatial variability due to nonhomogeneity of porous media, for example, formations with layers, lenses, etc. (e.g., in Jussel et al. 1994; Bayer et al. 2011). Moreover, it may show a directional behavior thus causing **anisotropic conditions**. Such conditions prevail, for example, in layered porous media where the largest hydraulic conductivity is parallel to the layering and the minimum hydraulic conductivity perpendicular to it (Figure 2.3). In general, formulation of the hydraulic conductivity coefficient is a symmetric second rank tensor (Bear 1979). Due to its symmetry, the number of components is six. For isotropic porous media, the tensor reduces to a single scalar quantity K_w. For anisotropic conditions, any symmetric tensor can be transformed into a diagonal matrix by rotation of the coordinate system by horizontal and vertical angles to the so-called **principal axes** x', y', and z', leading to the corresponding Darcy law with diagonal tensor:

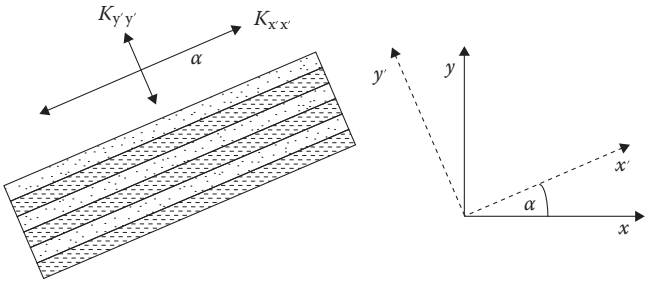

Figure 2.3 Inclined layer consisting of coarse (dotted) and fine (dashed) layers, leading to anisotropy in hydraulic conductivity of the layer as a whole; related coordinate systems with principal directions x' (parallel to the layering) and y' (perpendicular to layering).

$$\mathbf{q} = \begin{Bmatrix} q_x \\ q_y \\ q_z \end{Bmatrix} = -\mathbf{K}_w \nabla h_w = -\begin{bmatrix} K_{xx} & K_{xy} & K_{xz} \\ K_{yx} & K_{yy} & K_{yz} \\ K_{zx} & K_{zy} & K_{zz} \end{bmatrix} \begin{Bmatrix} \frac{\partial h}{\partial x} \\ \frac{\partial h}{\partial y} \\ \frac{\partial h}{\partial z} \end{Bmatrix} = -\begin{bmatrix} K_{x'x'} & 0 & 0 \\ 0 & K_{y'y'} & 0 \\ 0 & 0 & K_{z'z'} \end{bmatrix} \begin{Bmatrix} \frac{\partial h}{\partial x'} \\ \frac{\partial h}{\partial y'} \\ \frac{\partial h}{\partial z'} \end{Bmatrix} \tag{2.12}$$

Therefore, the number of essential components is reduced to three. In layered systems, it is often assumed that hydraulic conductivity that is parallel to layering is isotropic. Such a case can be described by one value parallel (maximum value) and one perpendicular to the layering (minimum value), one vertical angle of the layer plane with respect to the horizontal plane, and one horizontal angle defining the position of the plane. Moreover, very often, horizontal layering is observed in aquifers, thus reducing the hydraulic conductivity components to two, the horizontal and vertical hydraulic conductivities, that is, K_{hor}, and K_{vert}.

Unsaturated porous media are, in general, characterized by the presence of a continuous air phase besides a continuous water phase (Figure 2.2). Flow can take place in both fluid phases. The spatial distribution of both phases strongly depends on the wetting properties with respect to the solid phase (rock material). The volumetric fraction of both phases can be time dependent. The volumetric fraction of the water phase in a control volume is called **volumetric water content** θ_w (water volume per unit volume of porous medium). In unsaturated porous media, the volumetric water content θ_w is smaller than the **porosity** ϕ (interconnected pore volume per unit volume of porous medium). In a simplified manner, the water flux equation (Darcy's law) can be generalized from saturated flow conditions by analogy and adjusted accordingly. Consider the following situation. A vertical column with a homogeneous porous medium is recharged by a uniform steady-state infiltration rate at the top inflow face. If the column is long enough, practically uniform flow will be established with constant water content and constant (negative relative) water pressure, provided the infiltration rate is smaller than the hydraulic conductivity of the porous medium at saturation. Such a water flow system is characterized by two kinds of boundaries within the microscopic flow system. On the one hand, the solid phase represents the boundary as in saturated flow. On the other hand, the air–water interface is a boundary. The difference to saturated conditions lies in the fact that $\theta_w < \phi$. Furthermore, the resistance at the water–air interface is different. Even so, it can be presumed that **Darcy's law** for the water phase can be generalized for **constant water density** as follows (e.g., Bear 1979):

$$\mathbf{q}_w = -\mathbf{K}_w(S_w)\nabla\left(z + \frac{p_w}{\rho_w g}\right) \tag{2.13}$$

where S_w is the **water saturation**, with $S_w = \theta_w/\phi$. Still, it is formally equivalent to Equation 2.10. Similarly, Darcy's law for the air phase can be formulated correspondingly (Bear 1979). Moreover, it can be generalized according to Equation 2.2 in order to include density effects. It can be expected that **hydraulic conductivity strongly depends on the water saturation**, that is $\mathbf{K}_w(S_w)$, which is a phenomenological relationship with strongly decreasing hydraulic conductivity values for decreasing water saturation. Frequently used **models** for $\mathbf{K}_w(S_w)$ are those of Brooks and Corey (1966) and van Genuchten (1980). Brooks and Corey's model states that

$$K_w(S_w) = K_{w,sat}\left(\frac{S_w - S_{w,r}}{1 - S_{w,r}}\right)^{3+2/\lambda_{BC}} \tag{2.14}$$

where $S_{w,r}$ is the residual saturation (water saturation, which cannot be drained by gravitational effects only), $K_{w,sat} = K(S_w = 1)$, and λ_{BC} is the pore distribution index. Typical values in granular porous media are $S_{w,r} = 0.1$ and $\lambda_{BC} = 2$. Van Genuchten's (1980) model for $K_w(S_w)$ is

$$K_w(S_w) = K_{w,sat}S_{w,e}^{1/2}\left[1 - \left(1 - S_{w,e}^{1/m_{VG}}\right)^{m_{VG}}\right]^2 \tag{2.15}$$

With the parameters m_{VG}, n_{VG}, and $S_{w,r}$, and the effective water saturation $S_{w,e}$:

$$S_{w,e} = \frac{S_w - S_{w,r}}{1 - S_{w,r}} \tag{2.16}$$

Usually, $m_{VG} = 1 - 1/n_{VG}$. A modified formulation for improved description near saturation can be found in Schaap and van Genuchten (2006).

It is usually assumed in models that the relation $\mathbf{K}_w(S_w)$ is identical for static, steady-state, and transient conditions. Furthermore, hysteresis effects in $\mathbf{K}_w(S_w)$ are small and are often neglected. Therefore, the relation is considered unique.

2.1.1.2 Water mass balance, volume balance, flow equation

The general **mass balance for the water phase in a saturated porous medium** can be formulated for a unit control volume of the porous medium (Figure 2.4):

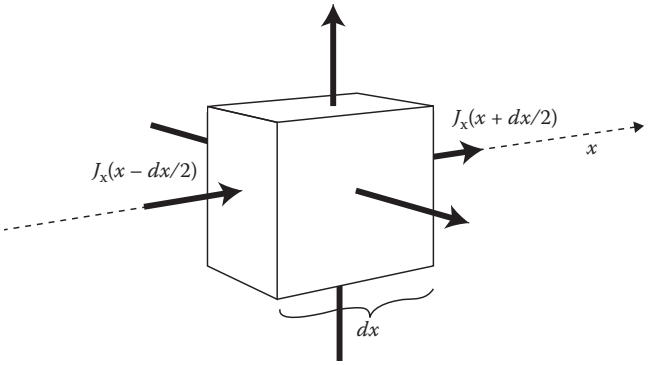

Figure 2.4 Unit control volume of a porous medium with flux components through horizontal fluxes in *x*-direction (schematic).

$$\frac{\partial(\phi\rho_w)}{\partial t} = -\nabla\cdot(\rho_w \mathbf{q}_w) + w\rho_w \tag{2.17}$$

where $\nabla\cdot()$ is the divergence operator, t is the time, and w is a hydraulic source/sink term (injection/extraction of water volume per unit volume of porous medium per unit time) (s^{-1}). Note that porosity $\phi(p_w(t))$ generally depends on water pressure and water density, while water density $\rho_w(p_w(t), T(t))$ depends on water pressure and temperature. The equation states that the rate of change of water mass over time equals water inflow minus outflow for a unit control volume. Assuming linear dependence of porosity from water pressure, that is, $\phi(p_w)$, according to

$$\phi(p_w) \simeq \phi(p_{w,0}) + a\,(p_w - p_{w,0}) \tag{2.18}$$

and by inserting in Equation 2.4, we obtain the following **water mass balance equation**:

$$\frac{\partial(\phi\rho_w)}{\partial t} = \phi\frac{\partial\rho_w}{\partial t} + \rho_w\frac{\partial\phi}{\partial t} = \left[(\rho_w(T)a + \rho_{w,0}\phi b_p)\frac{\partial p_w}{\partial t} + \rho_{w,0}\phi b_T\frac{\partial T}{\partial t}\right] \tag{2.19}$$

We may use the classical concept of **specific storativity** S_s (m^{-1}) with

$$S_s = (\rho_w a + \rho_{w,0}\,\phi b_p)g \tag{2.20}$$

and insert Darcy's law to obtain

$$\frac{S_s}{\rho_{w,0} g}\frac{\partial p_w}{\partial t} + \phi b_T \frac{\partial T}{\partial t} = \nabla\cdot\left[\mathbf{K}_w\left(\frac{\nabla p_w}{g\rho_{w,0}} + \nabla z + b_p \nabla z (p_w - p_{w,0}) + b_T \nabla z (T - T_0)\right)\right] + \frac{\rho_w(T)}{\rho_{w,0}} w \tag{2.21}$$

As an **alternative**, we can insert Equation 2.6 for the water density $\rho_w(T)$ and **Hubbert's** definition of a **water pressure–dependent piezometric head** $h_w(p_w)$, applied for isothermal conditions ($T = T_0$), with

$$h_w(p_w, T_0) = z + \int_{p_{w,0}}^{p_w} \frac{1}{\rho_w(p_w, T_0) g} dp_w \tag{2.22}$$

In the context of temperature-dependent flow, it can be considered as an **equivalent head**. With this formulation, the pressure gradient has the form

$$\nabla p_w = \rho_w(p_w, T_0) g \nabla h_w - \rho_w(p_w, T_0) g \nabla z \tag{2.23}$$

and the **water balance equation** is

$$S_s \frac{\partial h_w}{\partial t} + \phi b_T \frac{\partial T}{\partial t} = \nabla\cdot\left[\mathbf{K}_w(\nabla h_w + b_T \nabla z (T - T_0))\right] + \frac{\rho_w(T)}{\rho_{w,0}} w \tag{2.24}$$

This form was also presented by Mercer et al. (1982) and Clauser (2003). However, both start from the **equivalent piezometric head** h_w according to

$$h_w = z + \frac{p_w}{\rho_{w,0} g} \tag{2.25}$$

Molson et al. (1992) start from a simplified version for their model neglecting the second term in Equation 2.24 and obtain the water balance equation

$$S_s \frac{\partial h_w}{\partial t} = \nabla\cdot\left[\mathbf{K}(\nabla h_w + \rho_{rel}(T)\nabla z)\right] + w \tag{2.26}$$

with the **relative water density** $\rho_{rel}(T)$ according to

$$\rho_{rel}(T) = \frac{\rho_w(T)}{\rho_{w,0}} - 1 \tag{2.27}$$

The mass **balance for the water phase in unsaturated porous media with constant water density** ρ_w can be formulated as volume balance:

$$\phi \frac{\partial S_w}{\partial t} = -\nabla \cdot \mathbf{q}_w + w \tag{2.28}$$

The above formulation does not take into account compressibility effects of water and porous matrix, nor does it consider phase exchange processes between the phases, due to, for example, evaporation or condensation of water or air dissolution in water. Similarly, the mass balance for the air phase can be postulated correspondingly (Bear 1979). For saturated conditions, that is, $S_w = 1$, the transient term vanishes. By inserting Darcy's law into the volume balance equations and by **neglecting the influence of the air phase on water flow**, a nonlinear differential equation of second order, the **unsaturated flow equation**, also known as **Richards' equation,** is obtained:

$$\phi \frac{\partial S_w}{\partial t} = \nabla \cdot \left(\mathbf{K}_w(S_w) \nabla \left(z + \frac{p_w}{\rho_w g} \right) \right) + w \tag{2.29}$$

Neglecting air flow in the unsaturated zone means that air pressure is taken as atmospheric in the soil, with **zero relative air pressure**, that is, $p_a = 0$. Equation 2.29 contains the two variables S_w and p_w. Therefore, a further relation, the relation between water saturation S_w, the water pressure p_w, and the air pressure p_a, is required in order to solve the problem. The relation is known as the **water retention curve** $S_w(p_c)$, where p_c is called **capillary pressure**, with $p_c = p_a - p_w$ in general, or $p_c = -p_w$ when air flow is neglected (with $p_a = 0$). The water retention curve is a phenomenological relationship, with decreasing water saturation for decreasing water pressure values. Frequently used **models** for $S_w(p_c)$ are those of Brooks und Corey (1966) and van Genuchten (1980).

Brooks and Corey's model states that

$$\begin{aligned} S_{w,e} &= \frac{S_w - S_{w,r}}{1 - S_{w,r}} = \left(\frac{p_b}{p_c} \right)^{\lambda_{BC}}; \quad p_c \geq p_b \\ S_{w,e} &= 1; \qquad\qquad\qquad 0 \leq p_c \leq p_b \end{aligned} \tag{2.30}$$

where p_b is the air entry pressure (suction at which air enters the porous medium in drainage processes). The parameter λ_{BC} is the same as that used in Equation 2.14.

Van Genuchten's (1980) model for $S_{w,e}$ is

$$S_{w,e} = \frac{S_w - S_{w,r}}{1 - S_{w,r}} = \left(\frac{1}{\left(1 + \left| \alpha_{VG} \frac{p_c}{\rho_w g} \right|^{n_{VG}} \right)^{m_{VG}}} \right) \tag{2.31}$$

with the parameters m_{VG}, n_{VG}, and α_{VG}.

It is usually assumed in models that the relation $S_w(p_c)$ is identical for static, steady-state, and transient conditions. **Hysteresis effects** in $S_w(p_c)$ are present but are often neglected. Therefore, it is assumed that the relation is unique.

For **saturated conditions**, the flow Equation 2.17 for constant water density ρ_w but a compressible porous matrix is

$$S_s \frac{\partial h_w}{\partial t} = \nabla \cdot (\mathbf{K_w}(S_w) \nabla h_w) + w \tag{2.32}$$

The **specific storativity** S_s of the porous medium can be interpreted as water volume change in a unit control volume per unit change of the piezometric head h_w. For a more general discussion of saturated and unsaturated flow models, the reader is referred to Bear and Cheng (2010).

For **freezing soils and aquifers**, Equation 2.29 can be extended (Williams and Smith 1989; Hansson et al. 2004) for saturated and unsaturated conditions as follows:

$$\frac{\partial \theta_w}{\partial t} + \frac{\rho_i}{\rho_w} \frac{\partial \theta_i(T)}{\partial t} = \phi \frac{\partial S_w}{\partial t} + \frac{\rho_i}{\rho_w} \phi \frac{\partial S_i(T)}{\partial t} = \nabla \cdot \left[\mathbf{K}_w(p_w, T) \nabla \left(z + \frac{p_w}{\rho_w g} \right) \right] \tag{2.33}$$

where the subscript $_{-w}$ means liquid water, and θ_i and S_i are the volumetric ice content and the ice saturation. The second term on the left-hand side of Equation 2.33 expresses the rate of change of ice mass, measured as equivalent water volume, per unit time and unit volume. Flow (right-hand side) only occurs for liquid water. For the saturation degrees, the overall condition has to be fulfilled:

$$S_w + S_a + S_i = 1 \tag{2.34}$$

Equation 2.33 has to be coupled with the corresponding equation for heat transport, Equation 2.89.

2.1.1.3 Initial and boundary conditions

The **initial condition** for flow problems consists of specifying water pressure $p_w(\mathbf{x}, t = 0)$ in general, or piezometric head $h_w(\mathbf{x}, t = 0)$ for saturated zone models. The symbol $\mathbf{x}(x, y, z)$ denotes an arbitrary location vector.

Boundary conditions for flow problems are specified values of the variable at a boundary section B_1, specified water flux through a boundary section B_2, or flux through a semipermeable boundary section B_3.

Specified values p_{w1} or h_{w1} at a boundary section B_1 (Figure 2.5a) are, according to a first type or Dirichlet boundary condition:

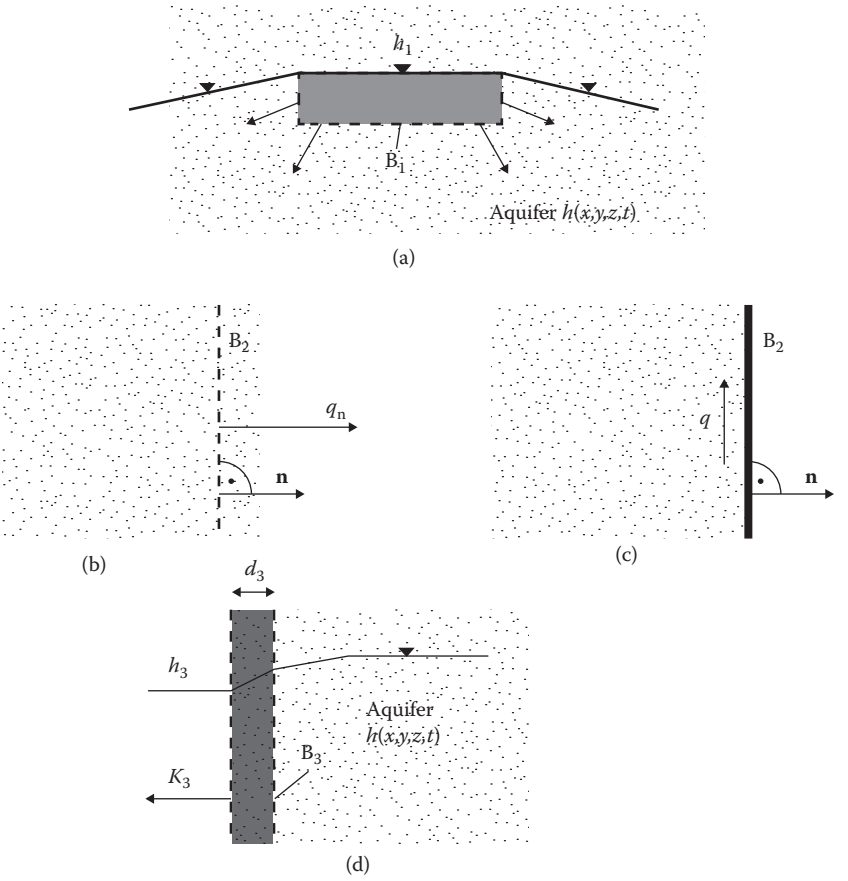

Figure 2.5 Hydraulic boundary conditions (schematic). (a) Surface water body with prescribed head, B_1; (b) prescribed flux into aquifer, B_2; (c) impermeable boundary, B_2; (d) semipermeable boundary, B_3.

$$p_w(\mathbf{x}_{B_1}, t) = p_{w_1}(\mathbf{x}_{B_1}, t); \quad \in B_1$$
$$h_w(\mathbf{x}_{B_1}, t) = h_{w_1}(\mathbf{x}_{B_1}, t); \quad \in B_1 \tag{2.35}$$

An example for B_1 is the direct connection of an aquifer with a surface water body at water level h_{w1}, thus controlling the water pressure in the adjacent aquifer.

Specified water flux $q_{w2,n}$ (normal component, positive in the direction of **n**) through a boundary section B_2 (Figure 2.5b), according to a second type or Neumann boundary condition, requires

$$q_{w,n}(\mathbf{x}_{B_2}, t) = q_{w_2,n}(\mathbf{x}_{B_2}, t) = \left(-K_{w,n} \frac{\partial h_w}{\partial n} \right)_{\mathbf{x}_{B_2}, t} \in \mathbf{B}_2 \tag{2.36}$$

An example for B_2 is a given infiltration rate through the soil surface, which eventually leads to recharge of the aquifer. Prescribed lateral inflow into an aquifer, for example, from hill slopes, or from an upstream valley, or prescribed inflow or extraction rates in boreholes and wells are some other examples. For an **impermeable boundary** (Figure 2.5c), $q_n = 0$.

The flux condition for a **semipermeable boundary** section B_3 (Figure 2.5d) in an isotropic aquifer is

$$-K_w \frac{\partial h_w}{\partial n}(\mathbf{x}_{B_3}, t) = K_3 \frac{\left[h_w(\mathbf{x}_{B_3}, t) - h_3 \right]}{d_3} = l_3 . \left[h_w(\mathbf{x}_{B_3}, t) - h_3 \right]; \quad \in B_3 \tag{2.37}$$

The symbol l_3 denotes the **leakage coefficient**. Note that for positive head gradients, the normal flux is directed from the solution domain to the outside region. The condition has the form of a mixed type or Cauchy boundary condition. An example for B_3 is a semipermeable river bottom, which exhibits reduced hydraulic conductivity values due to clogging effects caused by, for example, the deposition of fine sediments on the river bottom. The related additional resistance is accounted for by the leakage coefficient.

2.1.1.4 Two-dimensional flow models for saturated regional water flow

Regional water flow in shallow aquifers is frequently described by vertically averaged, two-dimensional horizontal flow models. This type of model is restricted to saturated conditions, where the aquifer thickness is small compared to the lateral extent. Consequently, vertical flow components are disregarded. The vertical integration of the flow equation for horizontally

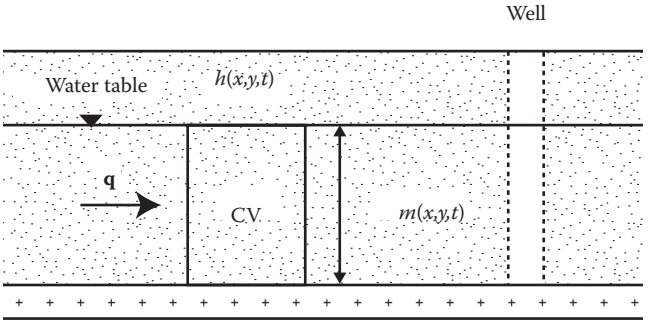

Figure 2.6 Schematic cross section through a shallow, extended, and unconfined aquifer, with control volume (CV) extending from aquifer bottom to the water table.

isotropic aquifers leads to the following **volume balance equation** for a control volume, based on Equation 2.32 (see Figure 2.6):

$$S\frac{\partial h_w}{\partial t} = \nabla\cdot(\mathbf{K}_w m \nabla h_w) + W \tag{2.38}$$

where S is the aquifer **storativity** (water volume change per unit horizontal area per unit change of piezometric head h_w). For confined aquifers, the storativity $S = S_s\, m$ is a small value, considering compressible deformation of water and porous matrix. For unconfined conditions, the coefficient is called **specific yield** or drainable porosity (water volume change per unit horizontal area per unit rise/decline of water table; usually smaller than porosity ϕ). The specific yield is usually much larger than the storativity of confined aquifers. The term ($\mathbf{K}_w\, m$) is called aquifer **transmissivity** (in general, a tensor), where m (m) is the **aquifer thickness**, which is, for unconfined aquifers

$$m(\mathbf{x}, t) = h_w(\mathbf{x}, t) - z_{bot}(\mathbf{x}) \tag{2.39}$$

The symbol $z_{bot}(\mathbf{x})$ denotes the **aquifer bottom elevation**. $W(\mathbf{x}, t)$ represents the source/sink term (water volume injection/extraction per unit area and per unit time) (m s^{-1}). This can be a **recharge term** $N(\mathbf{x}, t)$, or a local **source/sink,** such as a pumping well (discharge rate per unit area, Q/A). The aquifer thickness m is a function of the unknown flow variable $h_w(\mathbf{x},t)$. Equation 2.38 is therefore **nonlinear for unconfined aquifers**. For **confined aquifers**, the aquifer thickness is

$$m(\mathbf{x}) = z_{top}(\mathbf{x}) - z_{bot}(\mathbf{x}) \tag{2.40}$$

where z_{top} is the top of the aquifer. In this case, the volume balance equation is linear.

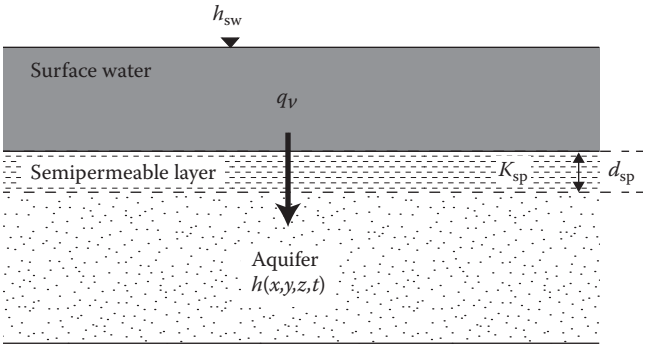

Figure 2.7 Semipermeable layer between surface water and aquifer (schematic cross section).

Interaction with surface water can be modeled by the local recharge term $N(\mathbf{x}_{sw})$ (m s^{-1}) for the horizontal area of the surface water body. In the case of a semipermeable layer (e.g., leaky rivers; Figure 2.7), this term is usually approximated by using Darcy's law for the vertical flux q_{vert}:

$$N_{sw} = q_{vert} = K_{sp} \frac{h_{sw} - h}{d_{sp}} = l(h_{sw} - h) \tag{2.41}$$

where K_{sp} is the hydraulic conductivity of the semipermeable layer, h_{sw} is the head of the surface water, d_{sp} is the thickness of the semipermeable layer, and l is the **leakage coefficient**. In the case where the groundwater table is below the bottom of the surface water, the vertical flux is usually approximated by

$$N_{sw} = q_{vert} = K_{sp} \frac{h_{sw} - z_{bot}}{d_{sp}} = l(h_{sw} - z_{bot}) \tag{2.42}$$

neglecting the water suction below the semipermeable layer. Note that in this case, a first-order term in $h_w(\mathbf{x})$ shows up in the flow Equation 2.38.

Initial and boundary conditions are formulated in a manner corresponding to the three-dimensional case.

2.1.2 Modeling thermal processes in porous media

Thermal processes in the subsurface essentially comprise heat conduction in solid materials (rock material, grains), in soil water, and in soil air, as well as heat advection in flowing water including thermal dispersion effects. In principle, they also include phase change processes (evaporation,

condensation, freezing, thawing), which are related to considerable energy transfers. However, for the thermal use of shallow subsurface systems, they are not usually significant and are, therefore, often disregarded. If, nevertheless, phase change processes have to be taken into account for a particular problem, the reader is referred to the literature of, for example, Williams and Smith (1989) for freezing soils. An introduction to heat transfer in fluids and solid materials can be found, for example, in Incropera et al. (2007). In these contexts, we will restrict ourselves to a brief introduction only.

2.1.2.1 Heat storage, heat capacity, and advective heat transport

The **thermal energy** ΔE (J) stored in a water volume V_w (m^3) at temperature T (°C), with respect to a reference temperature T_0, with $\Delta T = T - T_0$, can be expressed as follows:

$$\Delta E = V_w c_w \rho_w \Delta T \tag{2.43}$$

The coefficient c_w is the **specific heat capacity** (or specific heat) of water, which is related to a unit mass of water (J kg^{-1} K^{-1}). More precisely, it is the specific heat, which is usually determined for constant pressure conditions. The **volumetric heat capacity of water** C_w (J m^{-3} K^{-1}) related to a unit volume of water is

$$C_w = \rho_w c_w \tag{2.44}$$

The **reference temperature** T_0 can be, for example, the initial temperature or the mean annual temperature, or 0°C, depending on the situation to be investigated.

For **solid materials**, the specific heat capacity is, correspondingly, c_s, and the volumetric heat capacity C_s. In a similar manner, we get the specific heat capacity c_a and the volumetric heat capacity C_a for **air**.

For **saturated aquifer material** with porosity ϕ, the **volumetric heat capacity** C_m (J m^{-3} K^{-1}) is usually expressed by the **weighted arithmetic average** of the (mixed) values for water and solid material, weighted by the corresponding volumetric fractions:

$$C_m = \phi C_w + (1 - \phi) C_s \tag{2.45}$$

It represents the heat storage of water and solid matrix, presuming that the mean temperature for the water and the solid phase within a control volume are equal. For unsaturated conditions, with water, solid, and air as well as vapor phase, the volumetric heat capacity is, according to Whitaker (1977),

$$C_m = \phi S_w C_w + \phi S_a (C_a + C_v) + \phi S_i C_i + (1 - \phi) C_s \quad (2.46)$$

where $S_a = 1 - S_w - S_i$ is the air saturation, and C_a, C_v, and C_i are the volumetric heat capacities of air, vapor, and ice, respectively. However, the contribution of air and vapor is normally small and, therefore, often neglected. Values of volumetric heat capacities of water, sand packings, and aquifers are presented in Section 2.2.

Based on the storage concept, the **advective heat flux** J_w (J s^{-1}) for water flowing at the discharge rate Q ($m^3 s^{-1}$) and temperature T with respect to a reference temperature T_0 through a cross section can be expressed as

$$J_w = Q C_w (T - T_0) \quad (2.47)$$

Equation 2.47 applies for saturated and unsaturated conditions. The corresponding **specific advective heat flux** vector $\mathbf{j}_w$ (heat flux through unit area) (J m^{-2} s^{-1}) caused by the specific water flux vector $\mathbf{q}$ (Darcy flux) (m s^{-1}) is therefore

$$\mathbf{j}_w = \mathbf{q} C_w (T - T_0) \quad (2.48)$$

2.1.2.2 Heat conduction

The **heat flux** J_w **by heat conduction** (or thermal diffusion) through a cross section of water with area A in direction x normal to the area A is proportional to A and to the temperature gradient $\Delta T/\Delta x$:

$$J_{w,x} = A \lambda_w \frac{\Delta T}{\Delta x} \quad (2.49)$$

ΔT is the temperature increment over the spatial increment Δx. The coefficient λ_w is the **thermal conductivity of water** (W m^{-1} K^{-1}). Equation 2.49 is known as **Fourier's law**. The corresponding **specific heat flux vector** $\mathbf{j}_w$, assuming isotropic thermal conductivity, is

$$\mathbf{j}_w = -\lambda_w \nabla T \quad (2.50)$$

The specific heat flux $\mathbf{j}_s$ through a cross section of **solid material** is expressed in a similar manner, according to Fourier, as

$$\mathbf{j}_s = -\lambda_s \nabla T \quad (2.51)$$

using the thermal conductivity λ_s of solid material (rock material). For **aquifer material** consisting of water, rock, and air, the thermal conductivity λ_m

is an **equivalent parameter**, which is a function of the composition of solid material, water, and air. The corresponding heat flux vector is

$$\mathbf{j}_m = -\lambda_m \nabla T \tag{2.52}$$

Various techniques exist to express the thermal conductivity λ_m of saturated and unsaturated porous media, given values for water, ice, air, and rock material.

The simplest way to calculate the thermal conductivity consists of the **weighted arithmetic average** of thermal conductivities, according to Whitaker (1977):

$$\lambda_m = \phi S_w \lambda_w + \phi S_a \lambda_a + \phi S_i \lambda_i + (1 - \phi)\, \lambda_s \tag{2.53}$$

Again, the influence of the air phase is small. Usually, this value overpredicts the effective thermal conductivity of an aquifer. For **saturated porous media**, it is well known (see, e.g., Dagan 1989) that the **weighted arithmetic average** is the **upper bound** for the effective thermal conductivity (for $S_i = 0$):

$$\lambda_{m,\,sat} = \phi \lambda_w + (1 - \phi)\, \lambda_s \tag{2.54}$$

On the other hand, the **lower bound** is represented by the **weighted harmonic average**:

$$\lambda_{m,sat} = \frac{1}{\left[\dfrac{\phi}{\lambda_w} + \dfrac{(1-\phi)}{\lambda_s}\right]} \tag{2.55}$$

Dagan (1989) proposes the so-called **self-consistent approximation** (also termed renormalization approximation) to express thermal conductivity of saturated granular porous media ($S_w = 1$). The **effective thermal conductivity** is then

$$\lambda_{m,sat} = \frac{-b + \sqrt{b^2 + 8\lambda_w \lambda_s}}{4} \tag{2.56}$$

with the coefficient b

$$b = \lambda_w\,(3\phi - 1) - \lambda_s\,(2 - 3\phi) \tag{2.57}$$

Kunii and Smith (1960) derived equations to estimate the effective thermal conductivity $\lambda_{m,\,sat}$ of unconsolidated particle beds with uniform grain size distribution. For a porous medium saturated with water, $\lambda_{m,\,sat}$ is calculated as

$$\lambda_{m,sat} = \lambda_w \left[\phi + \frac{(1-\phi)}{\varepsilon + \frac{2}{3}\frac{\lambda_w}{\lambda_s}} \right] \tag{2.58}$$

The function ε depends on the effective thickness of water films adjacent to the contact surface of two solid particles and the number of contact points *n* of a particle with neighbors. It is determined by

$$\varepsilon = \frac{1}{3\kappa} \cdot \frac{\left(\frac{\kappa-1}{\kappa}\right)^2 \sin^2\alpha}{\ln(\kappa-(\kappa-1)\cos\alpha) - \frac{\kappa-1}{\kappa}(1-\cos\alpha)} \tag{2.59}$$

The symbol κ denotes $\kappa = \lambda_s/\lambda_w$. The angle α is determined by $\sin^2\alpha = 1/n$. The function ε is evaluated for both a loose packing ($\phi_1 = 0.476$) and the densest packing with uniform grains ($\phi_2 = 0.260$). The values for the corresponding number of contact points are $n_1 = 1.42$ and $n_2 = 6.93$. For arbitrary porosity, it is suggested that the function ε is determined by linear interpolation:

$$\begin{aligned} &\varepsilon = \varepsilon_2 \quad \text{for}\, \phi \le \phi_2; \\ &\varepsilon = \varepsilon_2 + (\varepsilon_1 - \varepsilon_2)\frac{\phi-\phi_2}{\phi_1-\phi_2} \quad \text{for}\, \phi_2 \le \phi \le \phi_1; \\ &\varepsilon = \varepsilon_1 \quad \text{for}\, \phi \ge \phi_1 \end{aligned} \tag{2.60}$$

de Vries (1963) proposed a method to calculate thermal conductivity of soils using volume fraction and physical properties of its constituents. His theory is based on Maxwell's approach and Burger's extension (Woodside and Messmer 1961) to calculate electrical conductivity of two-phase materials. For the extension, ellipsoidal soil particles with the axes *a*, *b*, and *c* are assumed, which are not in contact with each other and are embedded in a continuous medium of water. The effective **thermal conductivity** λ_m of a soil system consisting of *n* solid components is calculated as follows:

$$\lambda_m = \frac{\theta_w \lambda_w + \sum_{i=1}^{n} k_i \theta_i \lambda_i}{\theta_w + \sum_{i=1}^{n} k_i \lambda_i} \tag{2.61}$$

where $i = 1, n$ are soil components (mineral or organic soil particles), and θ_i is the volumetric fraction (with respect to unit soil volume). The weighting factors k_i are estimated from the shape of the particles and the thermal conductivities of water and the soil constituents:

$$k_i = \frac{1}{3}\left[\frac{1}{1+\left(\frac{\lambda_i}{\lambda_w}-1\right)g_a} + \frac{1}{1+\left(\frac{\lambda_i}{\lambda_w}-1\right)g_b} + \frac{1}{1+\left(\frac{\lambda_i}{\lambda_w}-1\right)g_c}\right] \tag{2.62}$$

where g_a is the shape factor of the ellipsoid in the a-direction. For spherical grains, the shape factors are $g_a = g_b = g_c = 1/3$. In this form, the equation corresponds to Maxwell's equation. The quantity k_i is conceived as the ratio of the average temperature gradients in the particles of types i and the corresponding quantity in the water. For the shape factors, de Vries (1963) used the theory of the dielectric constant as analogy. In general, the shape function g_a is found by the integral

$$g_a = \frac{abc}{2}\int_0^\infty \frac{du}{(a^2+u)^{3/2}(b^2+u)^{1/2}(c^2+u)^{1/2}} \tag{2.63}$$

The shape functions g_b and g_c are obtained in a similar manner, fulfilling the condition that $g_a + g_b + g_c = 1$. Unsaturated conditions can be considered in Equation 2.61 by treating the air as solid particles with the corresponding θ_a and λ_a. Woodside and Messmer (1961), Farouki (1981), Giakoumakis (1994), and Tarnawski and Wagner (1993) used the de Vries model successfully for their studies of unsaturated soils. However, it has to be noted that the de Vries model does not take into account nonuniform grain size distributions. Very often it is assumed that $g_a = g_b$. The value for g_c is $1–2g_a$. This leaves one value undetermined, which is often utilized as a fitting factor. Campbell et al. (1994) extended the de Vries theory and considered both the water and air phases as continuous functions by introducing a fluid thermal conductivity of the form

$$\lambda_f = \lambda_a + f_w (\lambda_w - \lambda_a) \tag{2.64}$$

where f_w is an empirical weighting function depending on the soil, which ranges from 0, in dry soils, to 1 in saturated soils.

In their laboratory experiments with unconsolidated packs of quartz grains, glass beads, and lead shot, **Woodside and Messmer** (1961) found that the formula of Maxwell underestimated the effective thermal conductivity. Both the approach of de Vries (1963) and of Kunii and Smith (1960) gave fair agreement with their observed data. This holds true also for the weighted geometrical mean model for the essential range of $\lambda_s/\lambda_w \leq 20$, which was also demonstrated by Menberg et al. (2013a) using various sands and silts from a well in Southern Germany.

Based on **Johansen's** (1975) model, **Farouki** (1981) suggested the following procedure. Thermal conductivity λ_m for porous media consisting of dry crushed rock material ($S_w = 0$) is empirically described by

$$\lambda_{m,\,dry} = (0.039\phi)^{-2.2} \tag{2.65}$$

and for natural soils

$$\lambda_{m,dry} = \frac{0.137\rho_b + 64.7}{2700 - 0.947\rho_b} \tag{2.66}$$

where ρ_b is the dry density of the packing. For saturated conditions ($S_w = 1$), the thermal conductivity λ_m of porous media is approximated by the **weighted geometric average** (Woodside and Messmer 1961) as follows:

$$\lambda_{m,sat} = \lambda_w^{\phi} \lambda_s^{(1-\phi)} \tag{2.67}$$

and for saturated, partially frozen soils

$$\lambda_{m,sat} = \lambda_w^{\theta_w} \lambda_i^{\theta_i} \lambda_s^{(1-\phi)} \tag{2.68}$$

where θ_w is the unfrozen volumetric water content, and θ_i is the volumetric ice content with the condition $\theta_w + \theta_i = \phi$. Thermal conductivity for wet material with water saturation S_w is interpolated according to Johansen (1975) as follows:

$$\lambda_m = \lambda_{m,\,dry} + (\lambda_{m,\,sat} - \lambda_{m,\,dry})\mathrm{Ke} \tag{2.69}$$

where the interpolation factor Ke is referred to as Kersten's number (Kersten 1949) and is empirically approximated for coarse mineral soils as

$$\mathrm{Ke} = 0.7 \log_{10}(S_w) + 1 \tag{2.70}$$

and for fine material

$$\mathrm{Ke} = \log_{10}(S_w) + 1 \tag{2.71}$$

According to Nield and Bejan (2006) and Menberg et al. (2013a), the weighted geometrical model (Equation 2.67) provides good results as long as the thermal conductivities of water and solids are not too different from each other. Farouki (1981) compared Johansens's model with data from experiments with fine soils and found good correspondence for saturated and unsaturated conditions.

Balland and Arp (2005) extended Johansen's (1975) method in order to **model thermal conductivity over a wide range of conditions**, from loose to compact, organic to mineral, fine to coarse textured, frozen to unfrozen, and dry to wet. They retained Equation 2.69 for the thermal conductivity of wet material and Equations 2.67 and 2.68 for saturated unfrozen and partially frozen conditions. The thermal conductivity of solid material is calculated as

$$\lambda_s = \lambda_{\mathrm{organic}}^{vf_{\mathrm{organic}}} \lambda_{\mathrm{quartz}}^{vf_{\mathrm{quartz}}} \lambda_{\mathrm{mineral}}^{vf_{\mathrm{mineral}}} \tag{2.72}$$

where vf_{organic}, vf_{quartz}, and vf_{mineral} are the volumetric fractions of organic material, quartz, and other minerals within the soil solids, respectively. Note that the thermal conductivity value for quartz is significantly higher than that of other typical minerals and organic matter. The **thermal conductivity for dry conditions** is determined as

$$\lambda_{\mathrm{dry}} = \frac{(0.053\lambda_s - \lambda_a)\rho_b + \lambda_a \rho_p}{\rho_p - (1 - 0.053)\rho_b} \tag{2.73}$$

where ρ_p and ρ_b are the particle and the bulk densities. For Kersten's number Ke in Equation 2.69, they offer the new **model for unfrozen soils**:

$$\mathrm{Ke} = S_{\mathrm{wi}}^{0.5(1+vf_{\mathrm{organic}}-\alpha vf_{\mathrm{sand}}-vf_{\mathrm{coarse}})} \left[\left(\frac{1}{1+\exp(-\beta S_{\mathrm{wi}})} \right)^3 - \left(\frac{1-S_{\mathrm{wi}}}{2} \right)^3 \right]^{1-vf_{\mathrm{organic}}} \tag{2.74}$$

where $S_{wi} = S_w + S_i$; S_i is the ice saturation; vf_{sand} and vf_{course} are the volumetric fractions of the sand and the coarse grain size fraction, respectively; and α and β are adjustable parameters. By model calibration using extensive data sets, Balland and Arp (2005) determined the parameters to be α = 0.24 ± 0.04, and β = 18.3 ± 1.1. Special importance has to be attached to the volumetric fractions $vf_{mineral}$ and vf_{quartz} within the soil solids. For frozen or partially frozen soil, Ke is

$$\mathrm{Ke} = S_{wi}^{1+vf_{organic}} \tag{2.75}$$

The model is valid for the temperature range from approximately –30°C to 30°C. Data on the thermal properties and densities of the basic soil constituents used in the model are presented in Table 2.1.

Chen (2008) investigated the effect of porosity and saturation degree on thermal conductivity of quartz sands through laboratory tests. He found that thermal conductivity increases with the decrease in porosity and the increase in saturation degree. An empirical equation of thermal conductivity expressed as a function of porosity and saturation degree was developed:

$$\lambda_m(\phi, S_w) = \lambda_s^{(1-\phi)}\lambda_w^{\phi}\left[(1-b)S_w + b\right]^{c\phi} \tag{2.76}$$

For saturated conditions, it reduces to the weighted geometrical mean model. From fitting with experimental data, Chen (2008) found $b = 0.0022$ and $c = 0.78$. On the other hand, Johansen's (1975) method gave a fair correspondence with his data.

Further expressions are offered for **frozen soil conditions** (Johansen 1975; Farouki 1981). Values on thermal conductivity of water, sand packings, and aquifers are, besides Table 2.1, presented in Section 2.2.

Overall, **a variety of methods and techniques have been proposed for the effective thermal conductivity.** Which model should be used might

Table 2.1 Thermal properties and densities of basic soil constituents after Balland and Arp (2005) for the use of their modified Johansen's method

Soil component	*Density (kg m^{-3})*	*Vol. heat capacity (J m^{-3} K^{-1})*	*Thermal conductivity (W m^{-1} K^{-1})*
Quartz	2660	2.01×10^6	8.0
Other mineral	2650	2.01×10^6	2.5
Organic matter	1300	2.51×10^6	0.25
Water	1000	4.18×10^6	0.57
Ice	920	1.88×10^6	2.21
Air	0.00125	1.25×10^3	0.025

indeed be confusing for the practitioner. In our opinion, it is important to take note of the existing attempts. Nevertheless, we may consider the approach of Balland and Arp (2005) as a good starting point for practitioners. However, this does not prevent us from critically assessing its validity under prevailing physical conditions. Moreover, existing codes may already contain specific approaches for the effective thermal conductivity.

2.1.2.3 Dispersive and macrodispersive heat transport

Similar to solute transport processes, **mechanical dispersion effects** in porous media may also play a role in thermal processes provided that significant flow is present. In a homogeneous porous medium, mechanical dispersion effects are again due to the highly variable microscopic velocity field. The related fluxes are essentially advective heat fluxes. The average advective thermal flux can be expressed by average values:

$$\overline{\mathbf{q}TC_w} = \overline{\mathbf{q}}\,\overline{T}C_w + \overline{\mathbf{q}'T'}C_w \tag{2.77}$$

where the overbar sign denotes the mean value within the control volume. The first term on the right-hand side corresponds to the advective thermal flux using mean values of specific water flux and temperature. Deviations from mean velocity and mean temperature within the control volume produce the **dispersive thermal heat flux** ($\overline{\mathbf{q}'T'}C_w$), which is furthermore influenced by heat diffusion effects in the flowing water, as well as the matrix. The **thermal mechanical dispersion effect** can be explained as follows. Consider a cross section in a pore. A water particle in the middle of a pore is transported with a much higher velocity downstream than a water particle close to the solid wall. This causes a pronounced longitudinal spreading effect of the fluid and therefore of the temperature after some transport time. A transversal dispersion effect is mainly due to the lateral detours of the water particles around grains or solid blocks in the porous medium. Anyway, both effects are further affected by thermal diffusion effects, mainly lateral heat conduction, within the pores and the matrix.

The **specific thermal flux due to mechanical dispersion** in porous media is usually approximated in analogy to Fick's or Fourier's law by

$$\mathbf{j}_{disp} = -\boldsymbol{\lambda}_{disp}\nabla T \tag{2.78}$$

for saturated conditions (Bear 1972; Green et al. 1964), where $\boldsymbol{\lambda}_{disp}$ is analogous to the combined medium λ_m. For unsaturated conditions, it is correspondingly

$$\mathbf{j}_{disp} = -\boldsymbol{\lambda}_{disp}(S_w)\nabla T \tag{2.79}$$

The coefficient λ_{disp} is the **thermal conductivity tensor due to mechanical dispersion.** For isotropic porous media, the tensor is expressed by the **longitudinal and the transversal thermal conductivity coefficients due to dispersion,** $\lambda_{disp,\,L}$, and $\lambda_{disp,\,T}$ (W m^{-1} K^{-1}), where the longitudinal direction equals the flow direction and the transversal direction is normal to the flow direction. Often, the effects of thermal conduction and mechanical thermal dispersion are combined to the equivalent or **effective thermal conductivity tensor** λ_{eff}, which has the following components in longitudinal (L) and transversal (T) directions:

$$\begin{aligned} \lambda_{eff,L} &= \lambda_m + \lambda_{disp,L} \\ \lambda_{eff,T} &= \lambda_m + \lambda_{disp,T} \end{aligned} \tag{2.80}$$

Note that the longitudinal dispersive flux component is formulated for the **mean direction of the groundwater flow.** Similarly, the transversal flux is expressed normal to the mean flow direction. If the x' axis of the coordinate system is chosen parallel to the flow direction in a **coordinate system with principal axes** x', y', z', the **effective thermal conductivity tensor** reads

$$\boldsymbol{\lambda}_{eff} = \begin{bmatrix} \lambda_{eff,xx} & \lambda_{eff,xy} & \lambda_{eff,xz} \\ \lambda_{eff,yx} & \lambda_{eff,yy} & \lambda_{eff,yz} \\ \lambda_{eff,zx} & \lambda_{eff,zy} & \lambda_{eff,zz} \end{bmatrix} = \begin{bmatrix} \lambda_{eff,x'} & 0 & 0 \\ 0 & \lambda_{eff,y'} & 0 \\ 0 & 0 & \lambda_{eff,z'} \end{bmatrix} = \begin{bmatrix} \lambda_{eff,L} & 0 & 0 \\ 0 & \lambda_{eff,T,hor} & 0 \\ 0 & 0 & \lambda_{eff,T,vert} \end{bmatrix} \tag{2.81}$$

Sometimes, the influence of thermal mechanical dispersion in homogeneous porous media is disregarded in theoretical studies (e.g., Bear 1972; Fujii et al. 2005; Woodbury and Smith 1985). This is motivated by the fact that the influence of thermal conductivity is often of similar magnitude to or larger than the thermal advection (Bear 1972; Woodbury and Smith 1985). Consequently, in thermal modeling, thermal dispersion is sometimes neglected (e.g., Domenico and Palciauskas 1973; Taniguchi et al. 1999; Reiter 2001; Ferguson et al. 2006).

The **effective thermal conductivity tensor** has been analyzed in a similar manner as the mechanical dispersion tensor for solute transport. Important parameters are the water velocity and the particle size of the porous medium (Green et al. 1964; Hsu and Cheng 1990; Levec and Carbonell 1985; Lu 2009; Metzger et al. 2004; Pedras and de Lemos 2008; Rau et al. 2012).

Metzger et al. (2004) investigated effective conductivity coefficients in laboratory experiments for packed beds (0.4 m long, 0.1 m wide) of glass beads (diameter 2 mm). They proposed the following correlation for the longitudinal and transversal effective thermal conductivity:

$$\lambda_{\text{eff,L}} = \lambda_{\text{m}} + b_{\text{L}}\lambda_{\text{w}}\text{Pe}_t^{m_{\text{L}}}$$
$$\lambda_{\text{eff,T}} = \lambda_{\text{m}} + b_{\text{T}}\lambda_{\text{w}}\text{Pe}_t^{m_{\text{T}}} \tag{2.82}$$

The dimensionless constant b_{L} is $b_{\text{L}} = 0.073$, the exponent m_{L} is $m_{\text{L}} = 1.59$, b_{T} is $b_{\text{T}} = 0.03–0.05$ (lower and upper limits), and $m_{\text{T}} = 1$. The dimensionless number Pe_{t} is the **thermal Peclet number**, which relates heat flux by advection to heat flux by conduction. It can be calculated as

$$\text{Pe}_{\text{t}} = \frac{C_{\text{w}} q d}{\lambda_{\text{m}}} \tag{2.83}$$

where d is a characteristic length, usually represented by the mean grain size. Equation 2.82 states that there is a **velocity dependence of the effective thermal conductivity coefficient**.

Rau et al. (2012) performed laboratory experiments on solute and heat transport in a homogeneous, well sorted quartz sand with a mean grain size of 2 mm. The chosen Darcy velocity range was 0.28 to 98 m day^{-1}. They found the following empirical formulae for the longitudinal and transversal effective thermal conductivity for their sand packing:

$$\lambda_{\text{eff,L}} = \lambda_{\text{m}} + \gamma_{\text{L}} \cdot C_{\text{m}} \left(\frac{C_{\text{w}}}{C_{\text{m}}} q \right)^2$$
$$\lambda_{\text{eff},T} = \lambda_{\text{m}} + \gamma_{\text{T}} \cdot C_{\text{m}} \left(\frac{C_{\text{w}}}{C_{\text{m}}} q \right)^2 \tag{2.84}$$

with the factors $\gamma_{\text{L}} \cong 1.478$ s and $\gamma_{\text{T}} \cong 0.4$ s. The effective thermal conductivity coefficient therefore approximately depends on the square of the Darcy velocity. For the solute transport experiments, on the other hand, they found a linear dependence of the solute dispersion coefficient from the flow velocity. The longitudinal solute dispersivity was 3 mm. In their analysis, they showed that the key element is the thermal Peclet number (Equation 2.83), which ranged from 0.02 to 3 in their study. This range shows a distinct **transitional behavior**, where both thermal conduction and advection are of similar magnitude. For very small flow velocities, a constant thermal conductivity coefficient applies. On the other hand, a linear relationship, where thermal advection clearly dominates, can be expected for very high flow velocities with a thermal Peclet number of about 10 and higher. However, according to the authors, this is unrealistic for most practical applications. One has to keep in mind that the relationship 2.84 is valid only for the chosen homogeneous quartz sand packing. Nevertheless,

it confirms the velocity dependence of the effective thermal conductivity tensor.

For geological formations, the dispersion phenomenon may be considerably affected and increased by **macrodispersion effects** due to the **high variability in hydraulic conductivity** (nonhomogeneous structures such as layers and lenses). Ferguson (2007) concluded from stochastic modeling based on geostatistical parameters that hydrodynamic macrodispersion is an important consideration in heat flow problems.

In order to **illustrate the macrodispersive heat flux** in a heuristic manner, we consider the simple extreme case of four horizontal layers as shown in Figure 2.8. The figure shows the vertical profile in the horizontal specific water flux $q(z)$ and the temperature profile $T(z)$ as a snapshot, assuming that flow of groundwater is horizontal and practically zero in two of the four layers with corresponding low temperature. Vertical heat flux is disregarded here. In this case, the total heat flux is easily calculated as $\overline{qT}C_w = 1$ unit, while the advective heat flux using mean hydraulic flux and mean temperature is $\overline{q}\,\overline{T}C_w = 0.5$ unit. Since the total flux $\overline{qT}$ can be expressed as $\overline{qT} = \overline{q}\,\overline{T} + \overline{q'T'}$, the macrodispersive flux can be calculated from the mean product of the deviations $q' = q - \overline{q}$, and $T' = T - \overline{T}$. The result is $\overline{q'T'}C_w = 0.5$ unit here. Therefore, the macrodispersive heat flux can be of the same order as the advective heat flux in extreme cases. This demonstrates the macrodispersion effect.

The **thermal macrodispersive flux** is again usually approximated by Equation 2.78. Similar to macrodispersion coefficients in solute transport, the **longitudinal and transversal thermal conductivity coefficients** are often

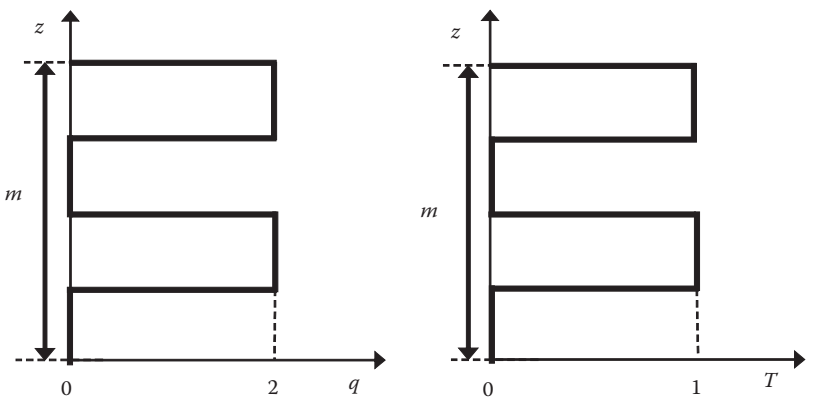

Figure 2.8 Example of a simple configuration with a layered aquifer and simple vertical specific flux and temperature profiles (schematic).

approximated by the Darcy velocity and by characteristic lengths in a linear manner:

$$\lambda_{\text{disp,L}} = \beta_{\text{L}} C_{\text{w}} q;$$
$$\lambda_{\text{disp,T}} = \beta_{\text{T}} C_{\text{w}} q \tag{2.85}$$

as suggested by Sauty et al. (1982) and adopted by de Marsily (1986). The parameters β_L (m) and β_T (m) are the **longitudinal and transversal thermal macrodispersivities**. The term $q = |\mathbf{q}|$ is the absolute value of the Darcy flux. The evaluation of field experiments in 1978, for the Bonnaud aquifer site in France (single and double well system, transport distance approximately 13 m), revealed that the longitudinal dispersivities seemed to be comparable for solute and heat transport (Sauty et al. 1982). Therefore, it is often assumed in numerical modeling that $\beta_L = \alpha_L$ and $\beta_T = \alpha_T$, where α_L and α_T (m) are longitudinal and transversal macrodispersivities, respectively, for solute transport (Smith and Chapman 1983; Molson et al. 1992; Hopmans et al. 2002; Constantz 2008).

From **analogy with solute transport** in nonhomogeneous formations (e.g., Dagan 1989), it can be expected that the **thermal macrodispersivities** behave in a similar manner. The spatially variable hydraulic conductivity field $K(\mathbf{x})$ can be described by a covariance function which depends on the variance σ_Y^2 and the correlation length I_Y (integral scale) of the spatial variable $Y = \ln(K(\mathbf{x}))$. Scale dependence of field-scale macrodispersivity values of tracer transport in various aquifers was demonstrated by Gelhar et al. (1992). It states that macrodispersivity values start from local mechanical dispersivity and typically grow with increasing transport scale, thus exhibiting a pronounced **scale effect**.

Vandenbohede et al. (2009) found in the analysis of their field experiment that the longitudinal dispersivities for solute and heat transport are not comparable. They performed two push–pull tests, injecting chloride and cold water into an aquifer using a single well. The mean radial transport distances for the tracer were up to about 11 m. They found that thermal dispersivities do not seem to be scale dependent. In this context, one has to keep in mind that the mean transport distances for tracers and heat are different, which is due to the different mean velocities for the thermal and the solute front.

Molina-Giraldo et al. (2011) presented values of longitudinal thermal macrodispersivity from the literature versus field scale together with empirical and semiempirical relationships for solute transport (Neuman 1990; Xu and Eckstein 1995; Schulze-Makuch 2005) (Figure 2.9). The relationships have the following general form:

$$A_{\text{L}} = bL^{m_2} \tag{2.86}$$

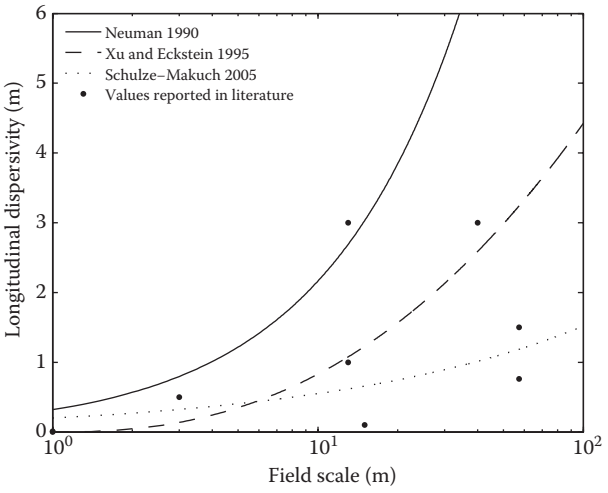

Figure 2.9 Longitudinal thermal macrodispersivity from the literature versus field scale together with empirical and semiempirical relationships for solute transport (Neuman 1990; Xu and Eckstein 1995; Schulze-Makuch 2005). (Modified after Molina-Giraldo, N. et al. *International Journal of Thermal Sciences* 50, 1223–1231, 2011.)

where b and m_2 are characteristic coefficients, and L is the length scale (advective transport distance). The data comprise evaluations from various unconsolidated aquifers worldwide. The longitudinal thermal dispersivity values clearly show scale effects. Measured values are best represented by the approach of Schulze-Makuch (2005). However, high variability for a given field scale is present, similar to the case of solute dispersivities shown by Gelhar et al. (1992). For a field scale of 10 m, for instance, the longitudinal dispersivity might be between 0.5 and 2 m. Nevertheless, most of the values are located within the ranges spanned by the empirical relationships. These differences reflect the specific geological conditions with respect to thermal dispersion effects.

Moyne et al. (2000) used stochastic concepts to express the development of the effective thermal conductivity in layered aquifers. **Hidalgo et al.** (2009) used a **stochastic approach** to describe heat transport in heterogeneous porous media, which is characterized by variance σ_Y^2 and correlation length I_Y. For steady-state conditions, longitudinal thermal dispersion is negligible, and the **transverse thermal dispersivity** is proportional to the variance of the log hydraulic conductivity Y and its correlation length I_Y, using a Gaussian covariance function as follows:

$$\beta_T = 0.02\sigma_Y^2 I_Y \tag{2.87}$$

As pointed out by Gelhar (1993), the correlation length I_Y of aquifers typically shows a distinct scale effect (typically 1/10 of the transport length scale).

Geiger and Emmanuel (2010) conducted numerical high-resolution finite element–finite volume simulations of heat transfer in two geologically realistic fractured porous domains. They calculated thermal breakthrough curves at various locations in the domains and analyzed them with a continuous time random walk (CTRW) model adapted for heat transfer. Their analysis shows that heat transport in the well-connected fracture network is Fourier-like, even though the thermal front is highly irregular. Consequently, it can be modeled by an advection–diffusion equation using macroscopic dispersivities. By contrast, heat transport in a poorly connected fracture pattern turned out to be highly non-Fourier-like. Hence, the classical advection–diffusion equation was not able to capture the main features, but they can be modeled successfully by CTRW. The authors conclude that the occurrence of non-Fourier behavior has important implications for a range of processes including geothermal reservoir engineering, radioactive waste storage, and enhanced oil recovery.

Chang and Yeh (2012) developed closed-form expressions using stochastic theory and the spectral perturbation techniques to describe the field-scale heat advection and the variability of the temperature profile in a partially saturated porous nonhomogeneous aquifer. Their results indicate that the macrodispersive heat flux depends on the spatial variability of the specific discharge, which, in turn, depends on the variation of hydraulic conductivity. The correlation length I_Y of log saturated hydraulic conductivity $Y(\mathbf{x})$ is important in enhancing the heat advection and the variability of the mean temperature field, and thus the macrodispersion effect. The longitudinal macrodispersivity value starts from a constant value and increases in an S-shaped manner over time or mean transport distance.

Nevertheless, the magnitude and development of the **effective thermal conductivity coefficient under field conditions are still a matter of debate** and have to be addressed in future research. In numerical models, however, **macrodispersion is usually taken into account with the help of constant (macro-)dispersivity values. Thermal dispersivity** values, which are only sparsely reported in the literature, are shown in Table 6.2.

A further physical effect, which is often modeled using a dispersion concept, is the **local temperature variation due to temporal variation of the flow field**, that is, nonpermanent flow direction and flow velocity. **Numerical simulations with solute transport in transient flow fields** have shown that considerable quasi-dispersive effects may occur. Kinzelbach and Ackerer (1986) showed that transversal dispersivity in contaminant transport is increased, and longitudinal dispersivity decreased in transient flow fields compared to steady-state ones. Dentz and Carrera (2005) showed

for heterogeneous hydraulic conductivity fields that stochastic longitudinal and transversal fluctuations of the hydraulic gradient can contribute to the effective dispersion coefficient even more strongly than macrodispersion does. It can be expected that **effects of transient flow fields are also relevant in heat transport**. Particularly long thermal plumes, which are modeled using mean velocity field, may thus exhibit considerable additional transversal dispersion effects.

2.1.2.4 Heat transport equation

Based on the expressions for storage of heat, advective heat flux, and heat conduction, including thermal macrodispersion effects and assuming that the mean temperatures of the water and the solid phase are the same within the control volume, the **energy balance for a unit volume of saturated or unsaturated porous medium** (Figure 2.4) can be formulated as

$$C_m \frac{\partial T}{\partial t} = \nabla \cdot \left[(\lambda_m + \boldsymbol{\lambda}_{disp}) \nabla T \right] - C_w \nabla \cdot (\mathbf{q} T) + P_t \tag{2.88}$$

where P_t is a thermal production term (heat production per unit volume and unit time) (W m^{-3}). The equation states that the rate of change of energy content equals the energy inflow minus the outflow over a unit control volume increased by the energy production in that volume. The assumption of equal mean temperature in water and solids of porous media is not exactly true at the microscopic level (Moyne et al. 2000).

If **freezing and thawing** are considered, the heat transport equation can be reformulated as follows (Williams and Smith 1989; Hansson et al. 2004):

$$C_m \frac{\partial T}{\partial t} - L_f \rho_i \frac{\partial \theta_i}{\partial t} = \nabla . \left[\boldsymbol{\lambda}(\theta_l, \theta_i) \nabla T \right] - C_w \nabla . (\mathbf{q}_w T) + P_t \tag{2.89}$$

where L_f (J kg^{-1}) is the latent heat of melting/freezing. The second term in Equation 2.89 represents the energy needed to melt the ice mass $\rho_i \theta_i$ per unit time and vice versa in the case of freezing. Note that this amount of energy is quite large (3.34×10^5 J kg^{-1}). In this case, the thermal conductivity also depends on the volumetric ice content. Here, it is assumed that the heat transport by air flow can be neglected. Still, a relationship is needed to fully define the systems. It is obtained by the **relationship between the liquid water pressure and temperature**, $p_w(T)$, for the absolute temperature $T < T_0$ (K), where T_0 is the freezing point temperature, in approximate form:

$$\frac{p_w}{\rho_w g} \simeq \frac{L_f (T - T_0)}{g T_0} \tag{2.90}$$

It is an application of the **principles of Clausius–Clapeyron on phase change parameters**. The **corresponding liquid water content** for freezing conditions is approximated using the relation between capillary pressure (i.e., water pressure p_w here with $p_a = 0$) and water saturation $S_w(p_w)$ of volumetric water content. For example, after Brooks and Corey (1966), the relation $\theta_w(T)$ is

$$\theta_w(T) = \theta_{w,r} + (\phi - \theta_{w,r})\left(\frac{h_b T_0 g}{(T_0 - T)}\right)^{\lambda_{BC}} \quad \text{for} \quad \frac{(T_0 - T)L_f}{T_0 g} > h_b \tag{2.91}$$

Although the liquid water saturation is extremely small for frozen conditions, it is still present.

Dividing the energy balance Equation 2.88 (without freezing/thawing) by the volumetric thermal capacity C_m and combining the effects of heat conduction and thermal macrodispersion in a thermal dispersion tensor $\mathbf{D}_t$ yields the **heat transport equation**

$$\frac{\partial T}{\partial t} = \nabla\cdot[\mathbf{D}_t \nabla T] - \frac{C_w}{C_m}\nabla\cdot(\mathbf{q}T) + \frac{P_t}{C_m} \tag{2.92}$$

Adopting a linear dependence of the macrodispersion coefficient on Darcy velocity, the **thermal diffusivity tensor** $\mathbf{D}_t$ in a hydraulically isotropic medium has the principal **longitudinal and transversal components**:

$$D_{t,L} = D_{t,diff} + D_{t,disp,L} = \frac{\lambda_m}{C_m} + \frac{\beta_L C_w |\mathbf{q}|}{C_m};$$
$$D_{t,T} = D_{t,diff} + D_{t,disp,T} = \frac{\lambda_m}{C_m} + \frac{\beta_T C_w |\mathbf{q}|}{C_m}; \tag{2.93}$$

The **thermal diffusion coefficient** $D_{t,diff} = \lambda_m/C_m$ ($m^2\ s^{-1}$) of a porous medium representing solely the effect of heat conduction is typically of the order of 10^{-7} to 10^{-6} $m^2\ s^{-1}$ for granular aquifers. This means that it is up to three orders of magnitude larger than the molecular diffusion coefficient. Therefore, thermal mechanical dispersion for homogeneous porous media is usually not dominant in heat transport problems. It may be of similar order of magnitude as thermal diffusion. Nevertheless, the effect of macrodispersion in nonhomogeneous aquifers is still present, as stated

above, depending on the prevailing macrodispersivity values. For typical situations, the macrodispersive flux dominates over the thermal diffusive flux due to heat conduction. Consequently, we keep the tensorial form of the heat transport equation.

We may compare the heat transport equation with the transport equation for a dissolved species with linear sorption and first order decay:

$$R_c \frac{\partial c}{\partial t} = \nabla \cdot \left[\mathbf{D}_h \nabla c \right] - \nabla \cdot [c\mathbf{u}] - \lambda_c R_c c \tag{2.94}$$

where R_c is the retardation factor (accounting for linear sorption effects), c (kg m^{-3}) is the solute concentration, $\mathbf{D}_h$ is the hydrodynamic dispersion coefficient (tensor) (m^2 s^{-1}), $\mathbf{u}$ (m s^{-1}) is the mean flow velocity vector ($\mathbf{u} = \mathbf{q}/\phi$), and λ_c (s^{-1}) is the decay coefficient. From the comparison, we can see that the variable T corresponds to c, the thermal diffusion tensor to the hydrodynamic dispersion tensor. The mean water velocity $\mathbf{u}$ corresponds to the **thermal velocity** $\mathbf{u}_t$ (m s^{-1}):

$$\mathbf{u}_t = \mathbf{q}\, C_w / C_m \tag{2.95}$$

This relation can be obtained by the advective thermal flux condition in porous media:

$$\mathbf{q} C_w (T - T_0)\ \mathbf{u}_t C_m (T - T_0) \tag{2.96}$$

As a consequence, when advective heat transport is dominant over heat conduction, a thermal front in groundwater propagates with the thermal velocity:

$$u_t = \frac{C_w \phi}{C_m} u \tag{2.97}$$

which is typically 2 to 3 times smaller than that for solute transport in granular aquifers. Therefore, a thermal front is retarded with respect to an ideal tracer front, with a **thermal retardation factor** R_{t_ret} [-] of

$$R_{t\_ret} = \frac{C_m}{\phi C_w} \tag{2.98}$$

Shook (2001) found that the **ratio of water to temperature velocity is constant, even for heterogeneous porous media.** Therefore, thermal breakthrough in heterogeneous media can be predicted from tracer tests. However, in the presence of strong permeability correlations, like in the case of layering, some deviations may occur.

Lo Russo and Taddia (2010) showed the prevalence of heat advective transport with respect to thermal dispersion for their field site in Torino, Italy. They investigated advective heat transport induced by the injection of an open-loop system. Thermal stratification was explained by prevailing horizontal advection of the flowing groundwater.

For **unsaturated conditions**, the porosity ϕ in Equations 2.97 and 2.98 has to be replaced by the water content $\theta_w = \phi S_w$. Note that according to Equation 2.46, the volumetric thermal capacity C_m depends on the water saturation S_w as well, which can be obtained from the solution of the flow problem. If uniform vertical flow conditions are assumed, the specific discharge q is constant and the vertical flow gradient is $I_{vert} = 1$ for homogeneous soils. We can therefore determine S_w using Equation 2.14 by setting $q = K_w(S_w)$ in this case. Unsaturated conditions can have quite some impact on the thermal front velocity.

For the modeler, it is important to know whether thermal macrodispersion dominates over heat conduction, or whether heat conduction dominates over heat advection. In the first case, the **ratio between dispersive and advective heat fluxes** can be expressed by the **dimensionless number**

$$\frac{\text{thermal dispersive flux}}{\text{flux by heat conduction}} = \frac{\beta_L C_w q}{\lambda_m} \tag{2.99}$$

Depending mainly on the longitudinal macrodispersivity and the Darcy flux values, the ratio indicates dominance of the respective term. The second case is described by the **thermal Peclet number** (Equation 2.83). For $Pe_t >> 1$, heat advection effects dominate over heat conduction. However, for **very small flow velocities** with $Pe_t << 1$, the heat transport Equation 2.92 reduces to the **heat conduction equation:**

$$C_m \frac{\partial T}{\partial t} = \nabla \cdot [\lambda_m \nabla T] + P_t \tag{2.100}$$

It can be written in the form of a diffusion equation (Carslaw and Jaeger 1959):

$$\frac{\partial T}{\partial t} = \nabla \cdot [D_t \nabla T] + P_t \tag{2.101}$$

where D_t is the thermal diffusion coefficient (scalar) with $D_t = \lambda_m / C_m$.

Characteristic quantities of thermal propagation, therefore, depend on the thermal Peclet number Pe_t. For very small Pe_t, the coefficients λ_m and C_m are needed. Characteristic parameters for larger Pe_t numbers are the **specific flux field q(x, *t*)** (Darcy flux), the **thermal capacity ratio** C_w/C_m,

and **the thermal diffusivity tensor $\mathbf{D}_t$**. The latter is typically dominated by macrodispersive effects characterized by the **longitudinal and transversal macrodispersivities** β_L and β_T. The ratio C_w/C_m is about 1.8 for granular aquifers. The **thermal conductivity** of porous materials λ_m is still needed to express boundary fluxes.

2.1.2.5 Initial and boundary conditions

The **initial condition for a heat transport problem** consists of a specified temperature distribution $T(\mathbf{x}, t = 0)$ for the whole solution domain.

Boundary conditions for heat transport problems are essentially specified values of the temperature T at a boundary section B_1, a specified conductive or convective–conductive heat flux through a boundary section B_2 or B_3. A further boundary consists of the outflow boundary B_4. All these sections are part of the boundary.

Specified temperature T_{B1} at a boundary section B_1 (first type or Dirichlet boundary condition; Figure 2.10a) is expressed by

$$T\left(\mathbf{x}_{B_1}, t\right) = T_{B_1}\left(\mathbf{x}_{B_1}, t\right); \quad \mathbf{x}_{B_1} \in B_1 \tag{2.102}$$

An example for B_1 is the infiltration zone from a surface water body at water temperature T_1 into the saturated or the unsaturated zone, or a borehole heat exchanger (BHE) with specified temperature. Another example is a soil surface with specified temperature. In this context, we have to be aware that the temperature at the soil surface, that is, just within the soil, is the result of a complex energy balance, taking into account input from shortwave and longwave radiation and outflowing longwave radiation (see Section 1.2.1), as well as fluxes into the ground caused by BHEs. Moreover, evaporation and transpiration effects occur as well as convective interactions with air and vapor flow close to the soil surface. Taking the resulting **soil surface temperature**, based on measurements, leads to a simplified formulation of the complex situation. It can be estimated using the relation with air temperature, as indicated in Section 1.2.1.

Specified conductive heat flux $j_{2,n}$ (normal component) through a boundary section B_2 requires (second type or Neumann boundary condition; Figure 2.10b)

$$j_n\left(\mathbf{x}_{B_2}, t\right) = -\lambda_n\left(\frac{\partial T}{\partial n}\right)_{B_2} = j_{2,n}\left(\mathbf{x}_{B_2}, t\right); \quad \mathbf{x}_{B_2} \in B_2 \tag{2.103}$$

The flux j_n is the thermal flux in the normal direction to the boundary surface, which is oriented from the solution domain to the outside. This means that for positive temperature gradients, it represents a thermal flux

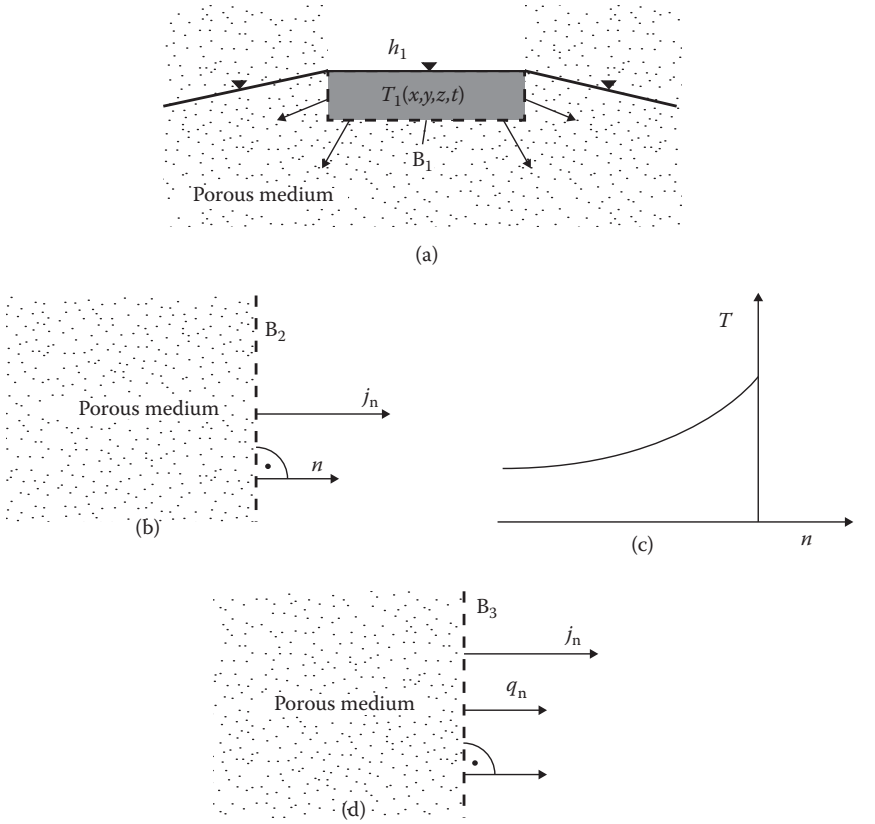

Figure 2.10 Thermal boundary conditions (schematic). (a) Surface water body with prescribed temperature, B_1; (b) specified conductive flux boundary, B_2; (c) temperature profile for solid material in contact with an outside fluid; (d) specified advective-conductive heat flux boundary, B_3.

out of the solution domain. An example for B_2 is a zone of specified conductive heat flux through the aquifer bottom, for example, by geothermal heat flux. A **thermally insulating boundary** is obtained by setting the condition $j_{2,n} = 0$.

For **solid materials** (e.g., solid wall) **in contact with an outside fluid** (e.g., air, or water), a mixed type (or third type or Cauchy boundary condition) is often applied, similar to Figure 2.10b and c (e.g., Gröber et al. 1955):

$$j_n\left(\mathbf{x}_{B_2},t\right) = -\lambda_n \cdot \left(\frac{\partial T}{\partial n}\right)_{B_2} = \alpha_t \cdot \left(T\left(\mathbf{x}_{B_2}\right) - T_{B_2}\right); \quad \mathbf{x}_{B_2} \in \mathbf{B}_2 \tag{2.104}$$

where T_{B2} is the temperature of the fluid outside of the thin thermal boundary layer close to the boundary, and α_t is the heat transfer coefficient (W K^{-1} m^{-2}). The latter coefficient depends on the flow conditions and state of the fluid.

Specified advective–conductive heat flux $j_{3,n}$ (normal component) through a boundary section B_3 requires (third type or Cauchy boundary condition; Figure 2.10d)

$$j_n\left(\mathbf{x}_{B_3},t\right)=q_n(T-T_0)-\lambda_n\left(\frac{\partial T}{\partial n}\right)_{B_3}=j_{3,n}\left(\mathbf{x}_{B_3},t\right);\quad \mathbf{x}_{B_3}\in B_3 \tag{2.105}$$

An example for B_3 is an inflow face of an aquifer with specified advective–conductive heat flux, or the borehole surface of a heat exchanger system where the heat flux is given. The role of the advective heat flux of infiltrating water is discussed in Kollet et al. (2009).

A further type of boundary condition concerns the **heat flux through the groundwater outflow face** of an aquifer (aquifer section B_4). The usual assumption of the heat insulation condition ($\partial T/\partial n$) = 0, where n is the normal direction to the outflow face, is often considered as unsatisfactory. An alternative is the establishment of the so-called **transmission boundary condition**, as sometimes used in solute transport models. The condition requires that the temperature gradient across the outflow boundary remains constant. This condition can be fulfilled in an approximate manner in numerical models by setting the dispersivity values to zero in the boundary cells.

In this context, we may pose the question about the **adequate thermal boundary conditions for technical systems** for the thermal use of aquifers. In the case of **open systems** with a defined inflow rate and temperature, the total inflowing borehole heat flux J_{bt} (W) (heat load) is specified. The specific heat flux can be related to a unit borehole length or borehole area.

For **closed systems** with BHEs, the steady-state total **borehole heat load** J_{bt} (W or J s^{-1}) is usually calculated using the mean temperature T_f (K) of the circulating fluid, the mean borehole surface temperature T_b (K), the length L (m) of the exchanger system, and a thermal borehole resistance R_t (K W^{-1} m^{-1}) as follows (e.g., Lamarche et al. 2010):

$$J_{bt}=\frac{L(T_f-T_b)}{R_t} \tag{2.106}$$

Various authors have proposed analytical and empirical approaches for the determination of the **thermal borehole resistance** (Lamarche et al. 2010; Wagner et al. 2013). The thermal resistance R_t depends on the specific geometrical configuration of the heat exchanger system (like vertical single U-tube borehole embedded in grouting material; Figure 1.8), the thermal

conductivity of soil, pipe, and borehole grouting material. Advective groundwater flow is usually disregarded. However, a recent study by Wagner et al. (2013) shows how groundwater-influenced thermal response tests (TRTs) in grouted BHEs with Darcy velocities > 0.1 m day^{-1} can be analyzed. The latter is comprehensively discussed in Chapter 6. Based on Equation 2.106 and depending on the mode of operation of the heat pump system, a **specified borehole temperature** or a **specified heat flux** at the borehole may be appropriate boundary conditions for the heat transport model. As pointed out by Wang et al. (2012), the **thermal performance** of heat exchanger systems in aquifers **with groundwater flow** may be strongly increased. They concluded from their case studies that the enhanced effect of the groundwater flow depends greatly on the amount, thickness, and depth of aquifers. The effect will mainly affect the mean borehole surface temperature T_b.

2.1.2.6 Concepts for BHEs

In order to implement the specific **design of BHEs** (single- or double-U-tube, coaxial BHE) into numerical models, various mathematical methods have been proposed. Since a detailed modeling of the complex three-dimensional BHE-aquifer systems including all processes in the inflowing and outflowing tubes and inside the borehole is cumbersome and time-consuming in practical applications, various concepts have been proposed in the past. Nevertheless, detailed numerical analyses have been performed for comparison and test purposes.

Consider a **single U-tube configuration** according to Figure 2.11. Both legs of the U-tube exhibit a different mean temperature within the tube, $T_{f1}(z, t)$ and $T_{f2}(z, t)$. The temperature at the borehole surface is $T_b(z, t)$

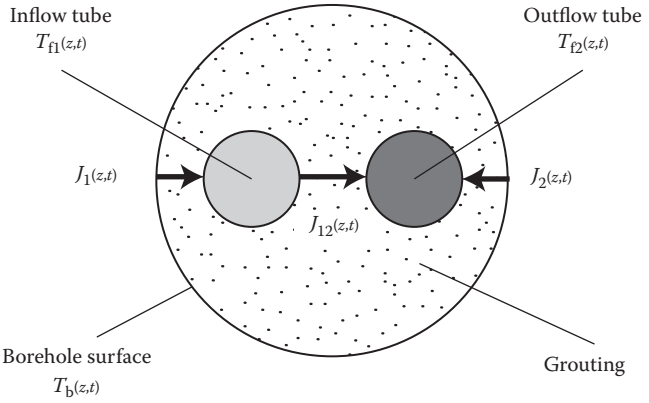

Figure 2.11 Single tube configuration with inflow and outflow tube. Schematic cross section at level z along the BHE.

neglecting axial temperature variation. The prevailing heat fluxes per unit length increment Δz are the heat fluxes from the borehole surface to each of the tubes and the heat fluxes between the tubes.

A widely used concept consists of relating the **heat flux from a cylindrical borehole wall to one single pipe**, which is embedded in grout material, to the **difference between the surface temperature of the borehole and the temperature of the fluid** circulating in the tube, together with a unit length thermal resistance R_t (see Section 2.1.2.5 and Equation 2.106). In the case of pipe 1, the heat flux is

$$J_1(z,t) = \frac{\left(T_b(z,t) - T_{f1}(z,t)\right)\Delta z}{R_{t1}} \tag{2.107}$$

where R_{t1} (K m W^{-1}) is the thermal resistance of pipe 1 including the grouting, and Δz (m) is a length increment along the borehole. The inverse of R_{t1} is related to a heat transfer coefficient. The other fluxes J_2 and J_{12} are formulated in a similar manner, with thermal resistance R_{t2} and R_{t12}. Equation 2.107 represents **a two-dimensional concept** in the plane normal to the axis of the BHE, valid for a particular location z along a vertical BHE at time t.

For such a single U-tube configuration, Eskilson and Claesson (1988) formulated the **heat balance in both tubes** as follows:

$$\begin{aligned}
\rho_f c_f Q_f \frac{\partial T_{f1}}{\partial z} &= \frac{J_1}{\Delta z} - \frac{J_{12}}{\Delta z} = \frac{T_b - T_{f1}}{R_{t1}} - \frac{T_{f1} - T_{f2}}{R_{t12}} \\
-\rho_f c_f Q_f \frac{\partial T_{f12}}{\partial z} &= \frac{J_2}{\Delta z} + \frac{J_{12}}{\Delta z} = \frac{T_b - T_{f2}}{R_{t2}} + \frac{T_{f1} - T_{f2}}{R_{t12}}
\end{aligned} \tag{2.108}$$

where Q_f (m^3 s^{-1}) is the pumping rate of the circulating fluid (heat carrier fluid). Heat capacity effects of all materials within the borehole and heat conduction in the axial direction are neglected. Equation 2.108 is valid along the vertical borehole and represents a coupled differential equation system. The **initial condition** is given by constant soil surface temperature and constant geothermal gradient. The **boundary condition** of the system is given by constant surface temperature and by specifying the inflow temperature $T_{f1}(z = 0, t)$. The constant soil surface temperature and the consideration of further boreholes are considered by using the superposition principle. The two pipes are connected at the **bottom of the borehole**, thus requiring equal temperature there. The term on the left-hand side in both equations denotes the rate of change of heat within the pipe per unit length of pipe due to heat advection within the pipe. The terms on the right-hand side are the heat fluxes from the borehole wall to the pipes and the heat flux between the pipes. All these heat fluxes are taken as quasi-steady fluxes,

thus disregarding heat capacity effects within the borehole. Therefore, the **timescale** has to be larger (Eskilson and Claesson 1988) than the timescale for thermal diffusion in the borehole and larger than the time needed for exchanging the fluid mass in the pipes:

$$\Delta t \geq \frac{5r_b^2}{D_t} + \frac{\pi r_p^2 2H}{Q_f} \tag{2.109}$$

where r_b (m) is the radius of the borehole, r_p (m) is the radius of the pipes, D_t is the thermal diffusion coefficient, and H is the length of the BHE. The **total heat flux along the borehole** can be expressed by

$$J_b(z,t) = \left(\frac{T_b - T_{f1}}{R_{t1}} + \frac{T_b - T_{f2}}{R_{t2}} \right) \Delta z \tag{2.110}$$

This heat flux along the borehole has to be coupled with the global heat transport outside the borehole.

Analytical solutions to equation system 2.108 are presented by Eskilson and Claesson (1988). The solution for $T_{f1}(z, t)$ and $T_{f2}(z, t)$ are related to the inflow temperature $T_{f1}(z = 0, t)$ and outflow temperature $T_{f2}(z = 0, t)$ of the fluids in the two pipes and the temperature profile $T_b(z, t)$ along the borehole. The temperature $T_{f2}(z = 0, t)$ yields the outflow temperature from the BHE.

Zeng et al. (2003) developed analytical solutions for the temperature profiles in the legs of single and double-U-tube BHE. They assumed that the borehole wall temperature T_b is invariant along the borehole depth but may change over time. Solutions (depending on T_1, T_2, and T_b) were developed for various combinations of the double U-tube for parallel and serial configurations.

Yang et al. (2009) combined the outside and inside regions of single U-tube configuration in an iterative manner. For the outside region, they used a cylindrical source model (Section 3.1.4).

For the **single, double U-tube, and the coaxial tube configurations**, related mathematical models were formulated by Diersch et al. (2011). They included transient heat storage, as well as thermal dispersion within the pipes. Still the thermal resistance concept is adopted. The grout material zone was subdivided into two (single U-tube) and four (double U-tube) subzones with corresponding grout temperatures. For quasi steady-state heat flux within the borehole, they provided **analytical solutions** analogous to Eskilson and Claesson (1988). According to Diersch et al. (2011), the analytical solutions strategy in the overall solution is highly efficient, precise, and robust. However, it is restricted to long-term processes, with timescales of the order of hours. They usually consider this limitation of

the analytical method to be irrelevant for real BHE applications, where the thermal process scales are measured in days and years. If finer temporal resolutions are required, a **numerical treatment of the transient system**, which is embedded in their finite element formulation for the aquifer, is feasible. Bauer et al. (2011) developed thermal resistance and capacity models for different types of BHEs. By considering the thermal capacity of the grouting material, a higher accuracy can be reached in transient simulations. This can be important, for example, in the case of TRTs. Bauer et al. (2011) checked their model against simulations using fully discretized finite element models. Zarrella et al. (2011) also extended the model for double U-tube configurations by considering thermal capacity of the grouting material in order to account for short-term analyses.

The unit length thermal resistance R_t depends on the geometrical configuration of the BHE, the thermal conductivity of the grout and pipe wall material, and heat conduction as well as heat convection effects within the pipe. It can be determined experimentally, empirically, or numerically or by analytical approximations. A review of thermal resistance formulations for the example of single U-tube configurations is given by Lamarche et al. (2010). Analytical expressions for the thermal resistance of single and double U-tube and coaxial configurations can be found in Diersch et al. (2011). Hellström (1991) and Claesson and Hellström (2011) developed the so-called multipole method to evaluate the thermal resistances between the heat carrier fluid in the pipes of the borehole and the immediate vicinity of the surrounding ground. Sagia et al. (2012) concluded from their numerical analysis that the borehole thermal resistance decreases as the spacing between GHE pipes increases, and that a rise in the thermal conductivity of the grout material leads to a decrease in the borehole resistance. Furthermore, a decrease in the pipe's diameter enables a decrease in the thermal resistance between the heat carrier fluid and the ground, and a small value of borehole thermal resistance is desirable in order to achieve a high performance of BHE systems. Based on their analytical model and Hellström's (1991) multipole solution for the thermal resistance, Zeng et al. (2003) expressed the effective borehole resistance. Their calculations show that the double U-tube boreholes are superior to those with the single U-tube with respect to the overall thermal resistance and that double U-tubes in parallel configuration show better performance than those in series. Jun et al. (2009) compared several thermal resistance models with data from a field study in Shanghai (China). They found that in their case, short-term thermal resistance is about 76% of the long-term resistance. Line-source and cylindrical source theory were successful as long as the thermal processes were conduction dominated. Based on a two-dimensional numerical analysis, Sharqawy et al. (2009) developed a correlation to express the effective borehole resistance, which deviates from current semianalytical models.

Marcotte and Pasquier (2008) showed in their numerical analysis that the **thermal resistance in borehole thermal conductivity tests** is overestimated when using the usually applied average temperature of the fluid entering and leaving the ground. They instead proposed a new estimator they termed "p-linear" using temperature variations to a power of $p \rightarrow -1$. The proposed p-linear average is

$$\left|\Delta T_p\right| = \frac{p\left(\left|\Delta T_{\text{in}}\right|^{p+1} - \left|\Delta T_{\text{out}}\right|^{p+1}\right)}{(1+p)\left(\left|\Delta T_{\text{in}}\right|^{p} - \left|\Delta T_{\text{out}}\right|^{p}\right)} \tag{2.111}$$

Sutton et al. (2003) developed a new ground resistance model for vertical BHEs with groundwater flow.

2.1.2.7 *Coupling thermal transport with hydraulic models*

In the case of **strong variability of water density and viscosity**, due to temperature fluctuations, the **water flow and the heat transport equations have to be solved simultaneously** in a coupled manner, because temperature changes, in general, affect water flow processes via temperature dependence on water density and viscosity. The related phenomenon of **density-driven flow** is **thermal convection** in porous media (e.g., Nield and Bejan 2006).

Considering the **flow Equation 2.24** for saturated aquifers:

$$S_{\text{s}} \frac{\partial h_{\text{w}}}{\partial t} + \phi b_{\text{T}} \frac{\partial T}{\partial t} = \nabla \cdot \left[\mathbf{K}_{\text{w}}(T)(\nabla h_{\text{w}} + b_{\text{T}} \nabla z \cdot (T - T_0))\right] + \frac{\rho_{\text{w}}(T)}{\rho_{\text{w},0}} w \tag{2.112}$$

and the **heat transport Equation 2.92**:

$$\frac{\partial T}{\partial t} = \nabla \cdot \left[\mathbf{D}_{\text{t}} \nabla T\right] - \frac{C_{\text{w}}}{C_{\text{m}}} \nabla \cdot (\mathbf{q}T) + \frac{P_{\text{t}}}{C_{\text{m}}} \tag{2.113}$$

It becomes evident that the head $h_{\text{w}}(\mathbf{x})$ and the flow field $\mathbf{q}(\mathbf{x})$ are temperature dependent and exhibit **possible density effects**, which in turn are used to evaluate heat transport. Nonlinearities exist in the temperature-dependent hydraulic conductivity $\mathbf{K}_{\text{w}}(\mathbf{x}, T)$ and the water density $\rho_{\text{w}}(\mathbf{x}, T)$.

For **small density differences**, the flow and the heat transport equations can be solved in an **uncoupled, sequential** manner.

Another type of coupling occurs at the soil surface. Parlange et al. (1998) demonstrated the **importance of advective water vapor transport to the mass and energy balance of diurnally heated soil surfaces of field soils**. This flux arises from the expansion and contraction of the soil air due to heating and

cooling over the day. Their analysis requires a coupled unsaturated water flow and a heat transport model that takes water vapor flux into account.

2.1.2.8 Two-dimensional heat transport models

The heat transport equation for **shallow regional aquifers** can be obtained by vertically integrating the three-dimensional equation according to the hydraulic case described in Section 2.1.1.2. The corresponding control volume extends, again, from the aquifer bottom to the water table according to Figure 2.6. Besides the horizontal thermal fluxes, the vertical fluxes through the bottom face and the top face of the control volume also have to be taken into account. These fluxes consist of the heat conduction flux through the bottom face and both the heat conduction and heat advection fluxes through the top face. However, because the fluxes through the top face will be highly transient over the year and difficult to express in detail, they might be represented in a simpler manner by considering yearly average conditions. Under these assumptions, **steady-state heat transport in shallow regional aquifers** (Figure 2.12) can be approximated by

$$\nabla\cdot(\mathbf{D}_t\nabla T)-\frac{C_w}{C_m}\nabla\cdot(\mathbf{q}T)+\frac{P_t}{mC_m}+\frac{j_{vert,bot}}{mC_m}+\frac{j_{vert,top}}{mC_m}=0 \qquad (2.114)$$

The parameter m is the aquifer thickness. The vertical thermal flux through the bottom face might be directly specified, possibly by the geothermal heat flux. The specific **vertical thermal flux through the top face** of the control volume can be approximated by linear expressions for the related conductive and advective fluxes:

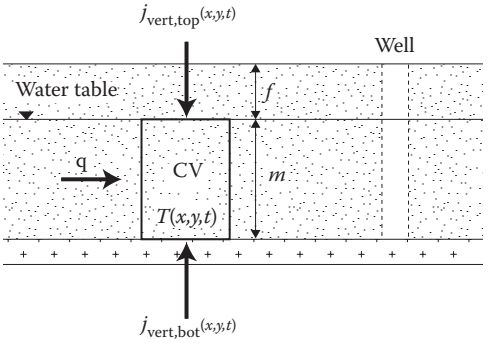

Figure 2.12 Schematic cross section through a shallow, extended unconfined aquifer, with control volume (CV) extending from aquifer bottom to the water table; thermal conditions.

$$j_{\text{vert,top}} \simeq \frac{\lambda_{\text{vert}}(T_{\text{surface}} - T)}{(f + m/2)} + NC_{\text{w}}(T_{\text{surface}} - T_0) \tag{2.115}$$

where λ_{vert} is an effective thermal conduction, expressing the thermal conductivity structure between soil surface and mean level of the saturated zone. The total thermal transfer distance therefore consists of the depth f to groundwater, and half the aquifer thickness, that is, $m/2$. The advective term depends on the mean (natural) recharge rate N (accretion rate, volume per unit area, and unit time).

Assuming, **for example**, an effective vertical thermal conductivity of $\lambda_{\text{vert}} = 2$ W m^{-1} K^{-1}, a depth to groundwater f of 5 m, an aquifer thickness m of 10 m, and a ΔT of 3 K, the related vertical conductive heat flux is $j_{\text{cond}} = 0.6$ W m^{-2}. The vertical advective heat flux j_{adv}, on the other hand, is for a mean recharge rate of 1 mm day^{-1} and the same ΔT, $j_{\text{adv}} = 0.15$ W m^{-2}. Therefore, vertical flux by heat conduction is dominant in this example.

2.1.3 Integral water and energy balance equations for aquifers

Integral balance equations for water and heat represent interesting tools for assessing and identifying the most important contributors in the context of the thermal use of shallow aquifers. However, in general, they do not replace the formulation of mathematical models, as described in Sections 2.1.1 and 2.1.2. Consider an aquifer domain D with saturated and possibly unsaturated zones. An integral water balance relates the rate of change of water volume within the domain D to all water fluxes in and out of it:

$$\frac{\mathrm{d}V_{\text{w}}}{\mathrm{d}t} = \sum_{i}^{M_{\text{w\_in}}} Q_{i\_\text{in}}(t) - \sum_{i}^{M_{\text{w\_out}}} Q_{i\_\text{out}}(t) \tag{2.116}$$

where $V_{\text{w}}(t)$ (m^3) is the water volume within the aquifer domain D, $Q_{i\_\text{in}}(t)$ (m^3 s^{-1}) are the inflow rates, $Q_{i\_\text{out}}(t)$ are the outflow rates (≤ 0), and $M_{\text{w\_in}}$ and $M_{\text{w\_out}}$ are the number of the inflowing and outflowing water flow components, respectively. A schematic example for an unconfined aquifer is shown in Figure 2.13. **Hydraulic inflow and outflow rates** Q_i can be listed as follows:

- Inflow $Q_{\text{sw\_in}}(t)$ from surface water bodies, like rivers and lakes
- Outflow $Q_{\text{sw\_out}}(t)$ from groundwater into surface water bodies
- Inflow $Q_{\text{replenish}}(t)$ from distributed natural replenishment at soil surface contributing to aquifer recharge
- Inflow $Q_{\text{lat\_in}}(t)$ through inflow into the aquifer from upstream regions, and lateral boundaries, including the aquifer bottom into the saturated or unsaturated zones of D

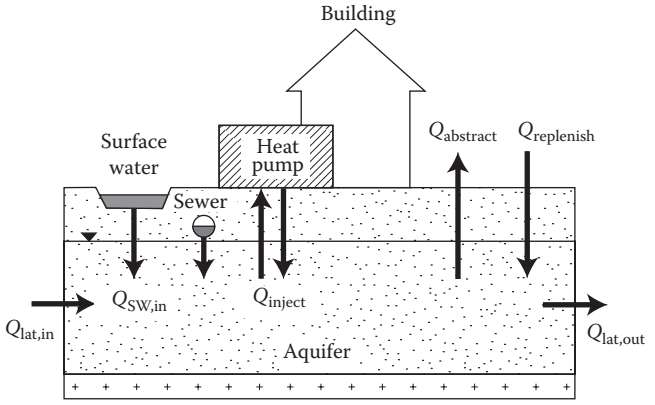

Figure 2.13 Hydraulic inflow and outflow rates for a schematic unconfined aquifer.

- Outflow $Q_{\text{lat\_out}}(t)$ from the aquifer into downstream regions, and from lateral boundaries including the aquifer bottom
- Water injection (inflow) $Q_{\text{inject}}(t)$, for example, by recharge wells, or infiltration by leaky sewers, or infiltration of roof water, or infiltration for thermal use
- Water abstraction (outflow) $Q_{\text{abstract}}(t)$, for example, by wells for drinking or process water use, or for thermal use

Note that **inflow is positive** and **outflow is negative**.

The **development of the integral water volume** in the aquifer over time can be formulated as follows:

$$V_{\text{w}}(t) = V_{\text{w0}}(t_0) + \sum_{i=1}^{M_{\text{w\_in}}} \int_{t_0}^{t} Q_{i\_\text{in}}(t)\,\mathrm{d}t + \sum_{i=1}^{M_{\text{w\_out}}} \int_{t_0}^{t} Q_{i\_\text{out}}(t)\,\mathrm{d}t \tag{2.117}$$

where V_{w0} is the initial water volume in the aquifer. In the **long run**, neglecting water volume changes for large values of time t, the water balance is simply

$$\sum_{i=1}^{M_{\text{w\_in}}} \overline{Q_{i\_\text{in}}} + \sum_{i=1}^{M_{\text{w\_out}}} \overline{Q_{i\_\text{out}}} = 0 \tag{2.118}$$

where $\overline{Q_i}$ are time-averaged rates, with

$$\overline{Q_i} = \frac{1}{t - t_0} \int_{t_0}^{t} Q_i(t)\,\mathrm{d}t \tag{2.119}$$

The rates $Q_i(t)$ have to be determined or estimated based on measurements or by modeling. The replenishment rate, for example, is calculated based on precipitation measurements minus modeled evapotranspiration (e.g., after Allen et al. 2006) and minus surface runoff. The flow from or into surface water bodies, with all the interactions between surface water and aquifer, is, in general, difficult to assess and usually requires two- or three-dimensional modeling using a calibrated groundwater flow model. Since we are primarily interested in average flow rates $\underline{Q}_i$, a steady-state model using time-averaged boundary conditions may be sufficient. The same holds true also for the lateral outflow rates from an aquifer, while inflow rates may be assessed by measurements and hydrological models.

An **integral heat balance** within the domain D can be formulated in a similar manner:

$$\frac{\mathrm{d}E}{\mathrm{d}t} = \sum_{i}^{M_{\mathrm{E\_in}}} J_{i\_\mathrm{in}}(t) + \sum_{i}^{M_{\mathrm{E\_out}}} J_{i\_\mathrm{out}}(t) \tag{2.120}$$

The balance equation relates the total energy $E(t)$ within the domain D to the heat fluxes $J_{i\_\mathrm{in}}(t)$ and $J_{i\_\mathrm{out}}(t)$ (W) in and out of the domain. $M_{\mathrm{E\_in}}$ and $M_{\mathrm{E\_out}}$ are the number of the inflowing and outflowing heat flow components, respectively. Schematically, the heat fluxes are included in Figure 2.14. The inflow and outflow rates $J_i(t)$ comprise, in principle, advective heat flow rates based on the prevailing water flow rates, supplemented by conductive heat flow rates. The **heat flow rates** can be listed as follows:

- Advective heat inflow rate $J_{\mathrm{sw\_in}}(t)$ from surface water bodies, like river and lakes

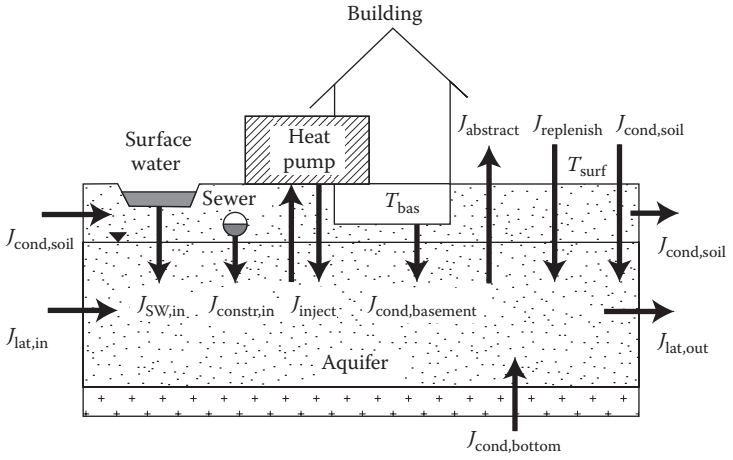

Figure 2.14 Thermal inflow and outflow rates for a schematic unconfined aquifer.

- Advective heat outflow rate $J_{sw\_out}(t)$ into surface water bodies
- Advective heat inflow rate $J_{replenish}(t)$ from distributed natural replenishment at soil surface or net loss due to areal evaporation or transpiration
- Advective lateral heat inflow rate $J_{lat\_in}(t)$ from upstream regions, or through lateral boundaries and the aquifer bottom into the saturated or unsaturated zones of domain D
- Advective lateral heat outflow rate $J_{lat\_out}(t)$ into downstream regions, or through lateral boundaries and the aquifer bottom into the saturated or unsaturated zones of domain D
- Advective heat inflow $J_{constr\_in}(t)$ from technical constructions (e.g., sewers, or infiltration of roof water, or from parking lots)
- Advective heat outflow $J_{constr\_out}(t)$ into constructions, like sewers
- Advective heat injection (inflow) $J_{inject}(t)$ from injection of heat by thermal use
- Advective heat abstraction (outflow) $J_{abstract}(t)$ from injection of heat by thermal use
- Conductive heat flow (inflow) $J_{cond\_soil}(t)$ through the soil surface into the domain D
- Conductive heat flow (inflow) $J_{cond\_lateral}(t)$ through the lateral boundaries and the bottom of the aquifer, into the domain D
- Conductive heat flow (inflow) $J_{cond\_constr}(t)$ from technical constructions (like sewers, or pipelines) into the domain D
- Conductive heat flow (inflow) $J_{cond\_basement}(t)$ from the basement of buildings into the domain D
- Heat injection (inflow) by BHEs, $J_{BHE\_in}(t)$
- Heat extraction (outflow) by BHEs, $J_{BHE\_out}(t)$

The **long-term heat balance** for the domain D, neglecting changes in energy storage within the aquifer for large values of time t, reads

$$\sum_{i=1}^{M_{w\_in}} \overline{J_{i\_in}} - \sum_{i=1}^{M_{w\_out}} \overline{J_{i\_out}} = 0 \tag{2.121}$$

where $\overline{J_i}$ are time-averaged rates, with

$$\overline{J_i} = \frac{1}{t - t_0} \int_{t_0}^{t} J_i(t)\,\mathrm{d}t \tag{2.122}$$

The heat flow rates $J_i(t)$ or directly $\overline{J_i}$ have to be calculated or estimated, again, using measurements and models, and the water flow rates are as determined above. The question of reference temperature T_0 may be raised

in this context. One possible reference temperature T_0 may be the average temperature $T_{surface}$ at the soil surface.

2.1.3.1 Rough estimation of the potential of an unconfined shallow aquifer for thermal use

A **simplified heat balance** can be obtained by considering long-term changes relative to a reference temperature T_0, and considering mean temperatures T_{gw} in shallow aquifers (saturated zone). Choosing the average temperature $T_{surface}$ at the soil surface as reference yields a relative temperature $T'(\mathbf{x}, t) = T(\mathbf{x}, t) - T_{surface}$, where T is the aquifer temperature. We further assume that the average temperature of surface water bodies is at the same reference temperature. With the relative temperature $T' = 0$ at the soil surface, and in the surface water bodies, the advective heat flow components J_{sw_in} and $J_{replenish}$, and possibly also the lateral component J_{lat_in}, may vanish depending on the thermal conditions. Furthermore, if the geothermal heat flux, as well as lateral heat advection, is neglected and no thermal use of the aquifer takes place, the groundwater temperature T_{gw} will also be at the relative temperature $T' = 0$. Now, we increase T_{gw} by ΔT due to thermal use, for example, due to the injection of warm water. A decrease ($\Delta T < 0$), on the other hand, will be obtained by the injection of cold water. For an increase of ΔT by the net heat fluxes from thermal use of groundwater J_{inject}, $J_{abstract}$, and J_{BHE}, the steady-state heat balance, neglecting conductive lateral heat fluxes, is

$$\overline{J_{sw\_out}} + \overline{J_{lat\_out}} + \overline{J_{constr\_out}} + \overline{J_{cond\_soil}} + \overline{J_{cond\_lat}} + \overline{J_{cond\_constr}} + \overline{J_{cond\_basement}} + \overline{J_{thermal\_use}} = 0 \tag{2.123}$$

Again, note that **inflow is positive** and **outflow is negative**.

The **potential heat flux** J_{pot} for optimal thermal use can be expressed by

$$\overline{J_{pot}} = \overline{J_{thermal\_use}} \tag{2.124}$$

The outflowing heat flux from surface water bodies $\overline{J_{sw\_out}}$, as well as $\overline{J_{lat\_out}}$, can be calculated based on the water outflow rate, for example, by modeling. Note that the sign of these rates depends on the sign of ΔT. For example, for $\Delta T < 0$, the advective heat outflow rate is negative. Heat flow from outflow into constructions J_{constr_out} or J_{cond_constr} might be small and can be roughly estimated. Lateral conductive heat transport J_{cond_lat} may diminish with time due to temperature equilibrium with the neighborhood of the

aquifer. Vertical conductive heat flux $\overline{J_{\text{cond\_soil}}}$ from the soil surface to the aquifer (see Figures 2.13 and 2.14) can be roughly estimated by

$$J_{\text{cond\_soil}} = A_{\text{soil}}\lambda_{\text{eff}}\frac{T_{\text{surface}} - T_{\text{gw}}}{\left(f + \frac{m}{2}\right)_{\text{soil}}} = A_{\text{soil}}\lambda_{\text{eff}}\frac{-\Delta T}{\left(f + \frac{m}{2}\right)_{\text{soil}}} \tag{2.125}$$

where λ_{eff} is the effective thermal conductivity for the section between soil surface and the mean level of the saturated zone, and A_{soil} is the surface area of the soil within the aquifer. It includes sealed surfaces. In a similar manner, the vertical conductive heat flux $\overline{J_{\text{cond\_basement}}}$ from the basements of buildings to the aquifer can be approximated by

$$J_{\text{cond\_basement}} = A_{\text{basement}}\lambda_{\text{vert}}\frac{T_{\text{basement}} - T_{\text{gw}}}{\left(f + \frac{m}{2}\right)_{\text{basement}}} \tag{2.126}$$

where A_{basement} is the integral area of basements from buildings.

Hötzl and Makurat (1981) and Menberg et al. (2013b) presented an example for a regional heat balance of an urban environment.

Consider an **illustrative, simple example** with a total area of 17 km^2, soil area A_{soil} = 14 km^2, mean distance of the soil from the aquifer $d = f + m/2$ = 12 m, and a total outflow rate of 0.7 m^3 s^{-1}. Vertical conductive heat flux $\overline{J_{\text{cond\_soil}}}$ from soil surface to the aquifer gets 7.0 MW, using an effective thermal conductivity of 2.0 W m^{-1} K^{-1} and a given temperature reduction of ΔT = –3 K. The vertical conductive heat flux from basements, with mean $d_{\text{\_basement}} = f + m/2$ = 10 m, $\overline{A_{\text{basement}}}$ = 3 km^2, and $T_{\text{basement}} - T_{\text{gw}}$ = 6 K, is 3.6 MW. The heat outflow rate $\overline{J_{\text{sw\_out}}}$ is –8.8 MW. Neglecting further heat fluxes results in a potential heat flux for maximum thermal use on the order of 19 MW. Of course, the energy potential provided by the reduction of the groundwater temperature, which can be accomplished only once, is additive (about 1700 TJ). A similar calculation can be performed for $\Delta T > 0$ (injection of warm water).

Keep in mind that the performance J_{pot} is a theoretical value, which is difficult to achieve in practice because of the interaction by many single thermal installations. More realistically, we may introduce an **energy utilization factor**, which denotes the fraction of the theoretical heat flux that is feasible to harness. This utilization factor is typically expected to be smaller than 0.5 (Zhu et al. 2010). Nevertheless, the potential heat flux J_{pot} provides an **upper limit of the long-term potential for thermal use**. Preferably the heat flux calculations are performed sector-wise to take into account mainly the variability of f and m within the total area.

2.2 THERMAL PROPERTY VALUES

2.2.1 Heat capacity and thermal conductivity values

The **specific heat capacity** c of a material (pure material like water or solid material) is defined as its increase (or decrease) in heat (energy) due to a unit increase (or decrease) in temperature, related to unit mass. Commonly used units are J kg^{-1} K^{-1} or W s kg^{-1} K^{-1}. An overview on the specific heat capacity of various minerals can be found in Waples and Waples (2004a,b) and Clauser (2011a). It can also be expressed as **volumetric heat capacity** C (also for mixtures, like soils) with commonly used units J m^{-3} K^{-1} or W s m^{-3} K^{-1}. The volumetric heat capacity C_m for soils or aquifers with porosity ϕ and water saturation S_w can be calculated using Equation 2.46. Similarly, the effective heat capacity of material with multiple components such as different minerals in soil is obtained by the volume-weighted mean of the individual fractions. Typically used values for thermal capacity of water, pure materials, and porous media from the literature are shown in Tables 2.1 through 2.6.

Table 2.2 Density, specific heat capacity, and thermal conductivity of water

Temperature (°C)	*Density*[a] ρ_w *(kg* m^{-3}*)*	*Specific heat capacity*[a] c_w *(J* kg^{-1} K^{-1}*)*	*Thermal conductivity*[b] λ_w *(W* m^{-1} K^{-1}*)*
0.1	999.84	4217.0	
5	999.97		0.5675
10	999.70	4190.6	0.5781
15	999.10		0.5881
20	998.21	4156.7	0.5975
25	997.05	4137.6	0.6064
30	995.65	4117.2	0.6147

[a] CRC 2011.
[b] Ramires et al. 1995.

Table 2.3 Volumetric heat capacity and thermal conductivity of soil for various water contents

Soil	θ_w *(*m^3 m^{-3}*)*	λ_m *(W* m^{-1} K^{-1}*)*	C_m *(J* m^{-3} K^{-1}*)*
Sandy soil (ϕ = 0.4)	0	0.3	1.28×10^6
	0.2	1.8	2.12×10^6
	0.4	2.2	2.96×10^6
Clay soil (ϕ = 0.4)	0	0.25	2×10^6
	0.2	1.18	3.10×10^6
	0.4	1.58	5.76×10^6

Source: After Williams, P.J. and Smith, M.W., *The Frozen Earth. Fundamentals of Geocryology*. Cambridge University Press, Cambridge, UK, 1989.

Table 2.4 Density, volumetric heat capacity, and thermal conductivity range of common aquifers and building materials

Material	ρ_m *(kg m^{-3})*	λ_m *(W m^{-1} K^{-1})*	C_m *(J m^{-3} K^{-1})*
Clay, silt, dry	1800–2000	0.4–1.0	1.5×10^6–1.6×10^6
Clay, silt, saturated	2000–2200	0.9–2.3	2.0×10^6–2.8×10^6
Sand, dry	1800–2200	0.3–0.8	1.3×10^6–1.6×10^6
Sand, saturated	1900–2300	1.5–4.0	2.2×10^6–2.8×10^6
Gravel, blocks, dry	1800–2200	0.4–0.5	1.3×10^6–1.6×10^6
Gravel, blocks, sat.	1900–2300	1.6–2.0	2.2×10^6–2.6×10^6
Clay, siltstone	2400–2600	1.1–3.5	2.1×10^6–2.4×10^6
Sandstone	2200–2700	1.3–5.1	1.8×10^6–2.6×10^6
Marble	2300–2600	1.5–3.5	2.2×10^6–2.3×10^6
Limestone	2400–2700	2.5–4.0	2.1×10^6–2.4×10^6
Dolomite	2400–2700	2.8–4.3	2.1×10^6–2.4×10^6
Granite	2400–3000	2.1–4.1	2.1×10^6–3.0×10^6
Bentonite		0.5–0.8	$\cong 3.9 \times 10^6$
Concrete	≅2000	0.9–2.0	$\cong 1.8 \times 10^6$
Steel	7800	60	3.12×10^6

Source: After VDI-Richtlinie 4640. Thermische Nutzung des Untergrundes (Guideline for thermal use of the underground). Verein Deutscher Ingenieure, VDI-Gesellschaft Energietechnik, Germany, 2012.

According to Fourier, **thermal conductivity** λ is the coefficient in the heat conduction equation. It expresses the ability of a material (pure material like water or solid material, or a mixture as present in soils) to conduct heat. The commonly used unit is W m^{-1} K^{-1}. Typically used values for the thermal conductivity of water, pure materials, and porous media from the literature are shown in Tables 2.1 through 2.6. An overview on the thermal conductivity of various rock material and minerals can be found in Waples and Waples (2004a,b), Clauser (2011b), and Banks (2008). Various models exist to express the heat thermal conductivity of soils or aquifers (Section 2.1.2.2). At this stage, we would like to recall the **arithmetic mean model** (Equation 2.54), the **harmonic mean model** (Equation 2.55), and the **geometric mean model** (Equation 2.67) for the thermal conductivity for saturated aquifer material with porosity ϕ. The coded functions (MATLAB scripts) of Equations 2.54, 2.55, and 2.67 can be found at http://www.crcpress.com/product/isbn/9781466560192 under the name "Tcond_arithmetic.m," "Tcond_harmonic.m," and "Tcond_geometric.m," respectively. A comparison of the results from the three models for a chosen porosity of $\phi = 0.25$ is depicted in Figure 2.15. It shows that, as expected, the arithmetic model represents the upper values and the harmonic model represents the lower ones, while the geometric model lies in between.

Table 2.5 Specific heat capacity and density of different soil-forming minerals and calculated volumetric heat capacities

Mineral groups	*Contents of groups*	*Density of Minerals* ρ_s *(kg m^{-3})*[a]	*Arithmetic average of density* ρ_s *(kg m^{-3})*	*Specific heat capacity of minerals* c_s *(MJ kg^{-1} K^{-1})*[b]	*Arithmetic average of specific heat capacity* c_s *(MJ kg^{-1} K^{-1})*	*Arithmetic mean of the volumetric heat capacity* C_s *of mixed minerals (J m^{-3} K^{-1})*
Tectosilicates Silica group	α-Quartz (trigonal) SiO_2	2650	2650	at 25°C, 0.74[c]	0.74	2×10^6
Tectosilicates Feldspar group	Albite $NaAlSi_3O_8$	2650	2600	0.71	0.77	2×10^6
	Anorthite $CaAl_2SiO_8$	2750		0.73		
	Oligoclase (Na, Ca) $(Si, Al)_4O_8$	2650		0.85		
	Orthoclase $KAlSi_3O_8$	2600		0.70		
	Microcline $KAlSi_3O_8$	2600		0.70		
Orthosilicates Olivine group	Fayalite Fe_2SiO_4	3400	3300	0.79	0.79	2.6×10^6
	Forsterite Mg_2SiO_4	3300		0.79		
	Monticellite $CaMgSiO_4$	3300		0.80		
Oxide group	Corundum Al_2O_3	4000	4800	0.71	0.71	3.4×10^6
	Hematite Fe_2O_3	5300		0.72		
	Magnetite Fe_3O_4	5100		0.70		
	Ilmenite $FeTiO_3$	4700		0.70		

(*continued*)

Table 2.5 (*Continued*) Specific heat capacity and density of different soil-forming minerals and calculated volumetric heat capacities

Mineral groups	*Contents of groups*	*Density of Minerals* ρ_s *(kg m^{-3})*[a]	*Arithmetic average of density* ρ_s *(kg m^{-3})*	*Specific heat capacity of minerals* c_s *(MJ kg^{-1} K^{-1})*[b]	*Arithmetic average of specific heat capacity* c_s *(MJ kg^{-1} K^{-1})*	*Arithmetic mean of the volumetric heat capacity* C_s *of mixed minerals (J m^{-3} K^{-1})*
Phyllosilicates Mica group (clay minerals)	Chlorite $(Mg, Fe)_3[(Si, Al)_4O_{10}[OH]_2]$	2800	2900	0.93	0.90	2.6×10^6
	Kaolinite	2700		0.95		
	Serpentine $(Mg, Fe)_3[Si_2O_5][OH]_4$	2900		1.00		
	Pyrophyllite $Al_2Si_4O_{10}[OH]_2$	2900		0.90		
	Biotite $K(Mg, Fe)_3(Al, Fe^{+3})Si_3O_{10}(OH, F)_2$	3000		0.80		
	Muscovite $KAl_2[Si_3Al]O_{10}[OH]_2$	2800		0.82		
Chain silicates Amphibole group	Actinolite $Ca_2(Mg, Fe)_5[Si_8O_{22}][OH]_2$	3100	3300	0.80	0.80	2.6×10^6
	Hornblende $Ca_2(Mg, Fe)_4(Al, Fe^{+3})[Si_7Al]O_{22}[OH]_2$	3300		0.84		
	Pargasite $NaCa_2(Mg, Fe)_4Al[Si_6Al_2]O_{22}[OH]_2$	3100		0.78		
	Rhodonite $(Mn^{2+}, Fe^{2+}, Mg, Ca)SiO_3$	3600		0.75		

Chain silicates Pyroxene group	Augite (Ca, Na)(Mg, Fe, Al, Ti)(Al, Si)$_2$O$_6$	3400	3300	0.75	0.77	2.6×10^6
	Diopside $CaMgSi_2O_6$	3400		0.77		
	Enstatite $Mg_2Si_2O_6$	3200		0.77		
	Jadeite Na(Al, Fe)Si_2O_6	3300		0.78		
Nonsilicates Sulfide group	Chalcopyrite $CuFeS_2$	4200	4800	0.53	0.45	2.2×10^6
	Sphalerite (Zn, Fe^{2+})S	4100		0.43		
	Arsenopyrite FeAsS	6000		0.43		
Nonsilicates Carbonate group	Calcite (trigonal) $CaCO_3$	2700	2750	0.80	0.88	2.4×10^6
	Dolomite $CaMg[CO_3]_2$	2800		0.91		

Source: Erol, S., Estimation of heat extraction rates of GSHP systems under different hydrogeological conditions, MSc. thesis, University of Tübingen, 85 pp., 2011.

Note: Thermal conductivity values are taken in a temperature range between 10°C and 35°C.

[a] Webmineral 2011.
[b] Clauser 2006.
[c] Grønvold et al. 1989.

Table 2.6 Calculated thermal properties of dry soils and rocks based on the mixed minerals

Mineral contents (%)[a]	*Selected soils and rocks*	*Region*[b]	*Volumetric heat capacity C_m of soils and rocks. Arithmetic average (MJ m^{-3} K^{-1})*	*Thermal conductivity λ_m of soils and rocks. Geometric average (W m^{-1} K^{-1})*
65% quartz, 20% potassium feldspar, 12% sodium feldspar, 1% muscovite, 1% biotite, 1% hornblende	Gneiss	Southeast Germany (Bayern)	2.1	4.4
35% K-feldspar, 30% plagioclase, 29% quartz, 5% biotite, 1% amphibole	Granite		2.0	3.2
43% plagioclase, 41% pyroxene, 5% alkali feldspar, 5% silica class, 5% olivine, 1% magnetite and ilmenite	Basalt		2.3	3.0
100% calcium and magnesium carbonates	Dolomite	Southwest Germany (Baden-Württemberg)	2.6	5.2[c]
100% calcite	Limestone		2.2	3.1[d]
50% quartz, 35% calcite, 13% plagioclase, 1% K-feldspar, 1% alkali feldspar	Gravel		2.0	4.5
90% quartz, 5% clay minerals, 5% K-feldspar	Sandstone	Middle Germany (Hessen)	2.0	5.5
90% clay minerals, 5% quartz, 3% carbonate, 1% feldspar, 1% sulfide	Clay	Northeast Germany (Brandenburg)	2.5	3.2
98% quartz, 1% feldspar, 1% clay minerals	Sand	North Germany (Mecklenburg Vorpommern)	2.0	6.0
60% quartz, 40% clay minerals	Silt	West Germany (Nordrhein-Westfalen)	2.2	4.6

Source: Erol, S., Estimation of heat extraction rates of GSHP systems under different hydrogeological conditions, MSc. thesis, University of Tübingen, 85 pp., 2011.

Note: The thermal conductivity and volumetric heat capacity of soils and rocks are taken for dry conditions.

[a] Press and Siever 1998.
[b] BGR 2011.
[c] VDI 2010.
[d] Thomas Jr. et al. 1973.

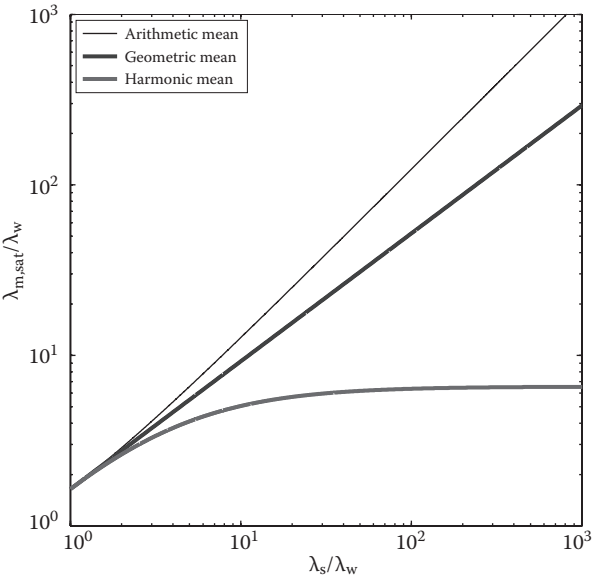

Figure 2.15 Comparison of the results from the three models "Tcond_arithmetic.m," "Tcond_harmonic.m," and "Tcond_geometric.m." (Modified after Woodside, W. and Messmer, J.H., *Journal of Applied Physics* 32 (9), 1688–1698, 1961.)

Markle et al. (2006) characterized thermal conductivity of a sand and gravel aquifer in Ontario, Canada, in detailed spatial resolution. They determined thermal conductivity values in a vertical two-dimensional profile by (1) measuring the thermal conductivity of solids and the mineral composition, (2) measuring the volumetric water content using cross-hole ground-penetrating radar, (3) evaluating several models for the effective thermal conductivity, (4) calculating the distribution using the selected model, and (5) simulating the thermal transport. The apparent thermal conductivity λ_m ranged between 2.14 and 2.69 W m^{-1} K^{-1} with a mean of 2.42 W m^{-1} K^{-1}. They found that the heterogeneous thermal conductivity field results in an increased thermal dispersion, which is most pronounced at the thermal front.

REFERENCES

Allen, R.G., Pereira, L.S., Raes, D., Smith, M. (2006). Crop evapotranspiration. Guidelines for computing crop water requirements. FAO Irrigation and Drainage Paper No. 56.

Balland, V., Arp, P.A. (2005). Modeling soil thermal conductivities over a wide range of conditions. *Journal of Environmental Engineering and Science* 4, 549–558, doi:10.1139/S05-007.

Banks, D. (2008). *An Introduction to Thermogeology: Ground Source Heating and Cooling*. Blackwell Publishing, Oxford, UK.
Bauer, D., Heidemann, W., Müller-Steinhagen, H., Diersch, H.-J.G. (2011). Thermal resistance and capacity models for borehole heat exchangers. *International Journal of Energy Research* 35, 312–320.
Bayer, P., Huggenberger, P., Renard, P., Comunian, A. (2011). Three-dimensional high resolution fluvio-glacial aquifer analog, Part 1: Field study. *Journal of Hydrology* 405, 1–9.
Bear, J. (1972). *Dynamics of Fluids in Porous Media*. Elsevier, New York, USA.
Bear, J. (1979). *Hydraulics of Groundwater*. McGraw-Hill, New York, USA.
Bear, J., Cheng, A.H.-D. (2010). *Modelling Groundwater Flow and Contaminant Transport*. Springer, Dordrecht, the Netherlands.
BGR (2011). Bundesanstalt für Geowissenschaften und Rohstoffe. Accessed on July 20, 2011, at http://www.bgr.bund.de.
Brooks, R.H., Corey, A.T. (1966). Properties of porous media affecting fluid flow. *Journal of the Irrigation and Drainage Division, Proceedings of the American Society of Civil Engineers ASCE* 92(2), 61–88.
Campbell, G.S., Jungbauer, J.D., Bidlake, W.R., Hungerford, R.D. (1994). Predicting the effect of temperature on soil thermal conductivity. *Soil Science* 158(5), 307–313.
Carslaw, H.S., Jaeger, J.C. (1959). *Conduction of Heat in Solids*. Oxford University Press, Oxford, UK.
Chang, C.-M., Yeh, H.-D. (2012). Stochastic analysis of field-scale heat advection in heterogeneous aquifers. *Hydrological Earth System Science HESS* 16, 641–648.
Chen, S.X. (2008). Thermal conductivity of sands. *International Journal of Heat and Mass Transfer* 44, 1241–1246.
Claesson, J., Hellström, G. (2011). Multipole method to calculate borehole thermal resistance in a borehole heat exchanger. *HVAC&R Research* 17(6), 895–911.
Clauser, C. (Ed.) (2003). *Numerical Simulation of Reactive Flow in Hot Aquifers—SHEMAT and Processing SHEMAT*. Springer, Berlin.
Clauser, C. (2006). Geothermal energy. In: K. Heinloth (Ed.), *Landolt-Börnstein—Numerical Data and Functional Relationships*. Springer Verlag, Heidelberg-Berlin.
Clauser, C. (2011a). Thermal storage and transport properties of rocks, I: Heat capacity and latent heat. In: H.K. Gupta (Ed.), *Encyclopedia of Solid Earth Geophysics*. 2nd ed., Springer, Dordrecht, pp. 1423–1431.
Clauser, C. (2011b). Thermal storage and transport properties of rocks, II: Thermal conductivity and diffusivity. In: H.K. Gupta (Ed.), *Encyclopedia of Solid Earth Geophysics*. 2nd ed., Springer, Dordrecht, pp. 1431–1448.
Constantz, J. (2008). Heat as a tracer to determine streambed water exchanges. *Water Resources Research* 44, W00D10, doi:10.1029/2008WR006996.
CRC (2011). *Handbook of Chemistry and Physics*. W.M. Haynes (Ed.), CRC Press, Boca Raton, FL, USA.
Dagan, G. (1989). *Flow and Transport in Porous Formations*. Springer, Berlin.
de Marsily, G. (1986). *Quantitavive Hydrogeology*. Academic Press, Orlando, USA.
Dentz, M., Carrera, J. (2005). Effective solute transport in temporally fluctuating flow through heterogeneous porous media. *Water Resources Research* 41, W08414, doi:10.1029/2004WR003571.

de Vries, D.A. (1963). Thermal properties of soil. In: W.R. van Wijk (Ed.), *Physics of Plant Environment*. North-Holland, Amsterdam, pp. 210–235.

Diersch, H.-J.G., Bauer, D., Heidemann, W., Rühaak, W., Schätzl, P. (2011). Finite element modeling of borehole heat exchanger systems. Part 1. Fundamentals. *Computer and Geosciences* 37, 122–1137.

Domenico, P.A., Palciauskas, V.V. (1973). Theoretical analysis of forced convective heat transfer in regional groundwater flow. *Geological Society of America Bulletin* 84(12), 3803–3814.

Erol, S. (2011). Estimation of heat extraction rates of GSHP systems under different hydrogeological conditions. MSc. thesis, University of Tübingen, Tübingen, Germany, 85 pp.

Eskilson, P., Claesson, J. (1988). Simulation model for thermally interacting heat extraction boreholes. *Numerical Heat Transfer* 13(2), 149–165.

Farouki, O.T. (1981). The thermal properties of soils in cold regions. *Cold Regions Science and Technology* 5, 67–75.

Ferguson, G. (2007). Heterogeneity and thermal modeling of ground water. *Ground Water* 45(4), 458–490.

Ferguson, G., Beltrami, H., Woodbury, A. (2006). Perturbation of ground surface temperature reconstructions by groundwater flow? *Geophysical Research Letters* 33, L13708, doi:10.1029/2006GL026634.

Fujii, H., Itoi, R., Fujii, J., Uchida, Y. (2005). Optimizing the design of large-scale ground-coupled heat pump systems using groundwater and heat transport modeling. *Geothermics* 34(3), 347–364.

Geiger, S., Emmanuel, S. (2010). Non-Fourier thermal transport in fractured geological media. *Water Resources Research* 46, W07504, doi:10.1029/2009WR008671.

Gelhar, L.W. (1993). *Stochastic Subsurface Hydrology*. Englewood Cliffs, New Jersey, Prentice-Hall.

Gelhar, L.W., Welty, C., Rehfeldt, K.R. (1992). A critical review of data on field-scale dispersion in aquifer. *Water Resources Research* 28(7), 1955–1974.

Giakoumakis, S.G. (1994). A model for predicting coupled heat and mass transfers in unsaturated partially frozen soil. *International Journal of Heat and Fluid Flow* 15(2), 163–171.

Green, D.W., Perry, R.H., Babcock, R.E. (1964). Longitudinal dispersion of thermal energy through porous media with a flowing fluid. *AIChE Journal* 10(5), 645–651.

Gröber, H., Erk, S., Grigull, U. (1955). *Grundgesetze der Wärmeübertragung*. U. Grigull (rev. ed.), Springer, Berlin, Germany.

Grønvold, F., Stølen, S., Svendsen, S.R. (1989). Heat capacity of [alpha] quartz from 298.15 to 847.3 K, and of [beta] quartz from 847.3 to 1000 K-transition behaviour and revaluation of the thermodynamic. *Thermochimica Acta* 139, 225–243.

Hansson, K., Šimůnek, J., Mizoguchi, M., Lundin, L.C., van Genuchten, M.T. (2004). Water and heat transport in frozen soils: Numerical solutions and freeze-thaw applications. *Vadose Zone Journal* 3, 693–704.

Hellström, G. (1991). Ground heat storage. Thermal analyses of duct storage systems. PhD Thesis, Lund University, Lund, Sweden.

Hidalgo, J.J., Carrera, J., Dentz, M. (2009). Steady state heat transport in 3D heterogeneous porous media. *Advances in Water Resources* 32(8), 1206–1212.

Hopmans, J.W., Simunek, J., Bristow, K.L. (2002). Indirect estimation of soil thermal properties and water flux using heat pulse probe measurements: Geometry and dispersion effects. *Water Resources Research* 38(1) 1006, 7-1–7-14, doi: 10.1029/2000WR000071.

Hötzl, H., Makurat, A. (1981). Veränderungen der Grundwassertemperaturen unter dicht bebauten Flächen am Beispiel der Stadt Karlsruhe. *Zeitschrift der deutschen geologischen Gesellschaft* 132, 767–777.

Hsu, C.T., Cheng, P. (1990). Thermal dispersion in a porous medium. *International Journal of Heat and Mass Transfer* 33(8), 1587–1597.

Incropera, F.P., Dewitt, D.P., Bergman, T.L., Lavine, A.S. (2007). *Introduction to Heat Transfer*. 5th ed., J. Wiley & Sons, Hoboken, NJ, USA.

Johansen, O. (1975). Thermal conductivity of soils. PhD thesis Univ. of Trondheim (Translation US Army Cold Regions Research and Engineering Laboratory, Hanover, NH, USA, 1977).

Jun, L., Xu, Z., Jun, G., Jie, Y. (2009). Evaluation of heat exchange rate of GHE in geothermal heat pump systems. *Renewable Energy* 34, 2898–2904.

Jussel, P., Stauffer, F., Dracos, T. (1994). Transport modeling in heterogeneous aquifer: 1. Statistical description and numerical generation of gravel deposits. *Water Resources Research* 30(6), 1803–1817.

Kersten, M.S. (1949). Final report, laboratory research for the determination of the thermal properties of soils. Corps of Engineers, US Army, Univ. Minnesota Engineering Experiment Station, Bulletin No. 28.

Kinzelbach, W., Ackerer, P. (1986). Modélisation de la proagation d'un contaminant dans un champ d'écoulement transitoire. *Hydrogéolgie* 2, 197–206.

Kollet, S.J., Cvijanovic, I., Schüttemeyer, D., Maxwell, R.M., Moene, A.F., Bayer P. (2009). The influence of rain sensible heat and subsurface energy transport on the energy balance at the land surface. *Vadose Zone Journal* 8(4), 846–857.

Kunii, D., Smith, J.M. (1960). Heat transfer characterristics of porous rocks. *AIChE Journal* 6(1), 71–78.

Lamarche, L., Kajl, S., Beauchamp, B. (2010). A review of methods to evaluate borehole thermal resistances in geothermal heat pump systems. *Geothermics* 39, 187–200.

Levec, J., Carbonell, R.G. (1985). Longitudinal and lateral thermal dispersion in packed beds. Part II. Comparison between theory and experiment. *AIChE Journal* 31(4), 591–602.

Lo Russo, S., Taddia, G. (2010). Advective heat transport in an unconfined aquifer induced by field injection of an open-loop groundwater heat pump. *American Journal of Environmental Sciences* 6(3), 253–259.

Lu, X. (2009). Experimental investigation of thermal dispersion in saturated soils with one-dimensional water flow. *Soil Science Society of America Journal* 73(6), 1912–1920.

Ma, R., Zheng, C. (2010). Effects of density and viscosity in modeling heat as a groundwater tracer. *Ground Water* 48(3), 380–389.

Marcotte, D., Pasquier, P. (2008). On the estimation of thermal resistance in borehole thermal conductivity tests. *Renewable Energy* 33, 2407–2415.

Markle, J.M., Schincarion, R.A., Sass, J.H., Molson, J.M. (2006). Characterizing the two-dimensional thermal conductivity distribution in a sand and gravel aquifer. *Soil Science Society of America Journal* 70, 1281–1294.

Menberg, K., Steger, H., Zorn, R., Reuß, M., Pröll, M., Bayer, P., Blum, P. (2013a). Bestimmung der Wärmeleitfähigkeit im Untergrund durch Labor- und Feldversuche und anhand theoretischer Modelle. *Grundwasser* 18(2), 103–116.

Menberg, K., Blum, P., Schaffitel, A., Bayer, P. (2013b). Long-term evolution of anthropogenic heat fluxes into asubsurface urban heat island. *Environmental Science and Technology*, in press.

Mercer, J.W., Faust, C.R., Miller, W.J., Pearson, F.J., Jr. (1982). Review of simulation techniques for aquifers thermal energy storage (ATES). In: V.T. Chow (Ed.), *Advances in Hydroscience* 13, 1–129. Academic Press, New York, USA.

Metzger, T., Didierjean, S., Maillet, D. (2004). Optimal experimental estimation of thermal dispersion coefficients in porous media. *International Journal of Heat and Mass Transfer* 47(14–16), 3341–3353.

Molina-Giraldo, N., Bayer, P., Blum, P. (2011). Evaluating the influence of thermal dispersion on temperature plumes from geothermal systems using analytical solutions. *International Journal of Thermal Sciences* 50, 1223–1231.

Molson, J.W., Frind, E., Palmer, C.D. (1992). Thermal energy storage in an unconfined aquifer: 2. Model development, validation, and application. *Water Resources Research* 28(10), 2857–2867.

Moyne, C., Didierjean, S., Amaral Souto, H.P., da Silveira, O.T. (2000). Thermal dispersion in porous media: One-equation model. *International Journal of Heat and Mass Transfer* 43(20), 3853–3867.

Neuman, S.P. (1990). Universal scaling of hydraulic conductivities and dispersivities in geologic media. *Water Resources Research* 26(8), 1749–1758.

Nield, D.A., Bejan, A. (2006). *Convection in Porous Media*. Springer, New York, USA.

Oostrom, M., Hayworth, J.S., Dane, J.H., Güven, O. (1992). Behavior of dense aqueous phase leachate plumes in homogeneous porous media. *Water Resources Research* 28(8), 2123–2134.

Parlange, M.B., Cahill, A.T., Nielsen, D.R., Hopmans, J.W., Wendroth, O. (1998). Review of heat and water movement in field soils. *Soil and Till Research* 47, 5–10.

Pedras, M.H.J., de Lemos, M.J.S. (2008). Thermal dispersion in porous media as a function of the solid-fluid conductivity ratio. *International Journal of Heat and Mass Transfer* 51(21–22), 5359–5367.

Press, F., Siever, R. (1998). *Understanding Earth*. 2nd ed., W.H. Freeman, New York.

Ramires, M.L.V., Nieto de Castro, C.A., Nagasaka, Y., Nagashima, A., Asseql, M.J., Wakeham, W.A. (1995). Standard reference data for the thermal conductivity of water. *Journal of Physical and Chemical Reference Data* 24(3), 1377–1381.

Rau, G., Andersen, M.S., Acworth, R.I. (2012). Experimental investigation of the thermal dispersivity term and its significance in the heat transport equation for flow in sediments. *Water Resources Research* 48, W03511, doi:10.1029/2011WR011038.

Reiter, M. (2001). Using precision temperature logs to estimate horizontal and vertical groundwater flow components. *Water Resources Research* 37(3), 663–674.

Sagia, Z., Stegou, A., Rakopoulos, C. (2012). Borehole resistance and heat conduction around vertical ground heat exchangers. *The Open Chemical Engineering Journal* 6, 32–40.

Sauty, J.P., Gringarten, A.C., Fabris, H., Thiery, D., Menjoz, A., Landel, P.A. (1982). Sensible energy storage in aquifers 2. Field experiments and comparison with theoretical results. *Water Resources Research* 18(2), 253–265.

Schaap, M.G., van Genuchten, M.T. (2006). A modified Mualem–van Genuchten formulation for improved description of the hydraulic conductivity near saturation. *Vadose Zone Journal* 5, 27–34.

Schulze-Makuch, D. (2005). Longitudinal dispersivity data and implications for scaling behaviour. *Ground Water* 43(3), 443–456.

Sharqawy, M.H., Morkheimer, E.M., Bader, H.M. (2009). Effective pipe-to-borehole thermal resistance for vertical ground heat exchangers. *Geothermics* 38, 271–277.

Shook, M. (2001). Predicting thermal breakthrough in heterogeneous media from tracer tests. *Geothermics* 30, 573–589.

Smith, L., Chapman, D.S. (1983). Thermal effects of groundwater flow. 1. Regional scale systems. *Journal of Geophysical Research* 88(B1), 593–608.

Sutton, M.G., Nutter, D.W., Couvillion, R.J. (2003). A ground resistance for vertical bore heat exchangers with groundwater flow. *Journal of Energy Resources Technology ASME* 125(3), 183–189.

Taniguchi, M., Shimada, J., Tanaka, T., Kayane, I., Sakura, Y., Shimano, Y., Dapaah-Siakwan, S., Kawashima, S. (1999). Disturbances of temperature-depth profiles due to surface climate change and subsurface water flow: 1. An effect of linear increase in surface temperature caused by global warming and urbanization in the Tokyo metropolitan area, Japan. *Water Resources Research* 35(5), 1507–1517.

Tarnawski, V.R., Wagner, B. (1993). Modeling the thermal conductivity of frozen soils. *Cold Regions Science and Technology* 22, 19–31.

Thomas, J., Jr., Frost, R.R., Harvey, R.D. (1973). Thermal conductivity of carbonate rocks. *Engineering Geology* 7(1), 3–12.

van Genuchten, R. (1980). A closed form equation for predicting the hydraulic conductivity of unsaturated soils. *Soil Science Society of America Journal* 44, 892–898.

Vandenbohede, A., Louwick, A., Lebbe, L. (2009). Conservative solute vs. heat transport in porous media during push-pull tests. *Transport in Porous Media* 76, 265–287.

VDI (2012). VDI-Richtlinie 4640: Thermische Nutzung des Untergrundes (Guideline for thermal use of the underground). Verein Deutscher Ingenieure, VDI-Gesellschaft Energietechnik, Germany.

Wagner, V., Blum, P., Kübert, M., Bayer, P. (2013). Analytical approach to groundwater-influenced thermal response tests of grouted borehole heat exchangers. *Geothermics* 46, 22–31.

Wang, H., Yang, B., Xie, J., Qi, C. (2012). Thermal performance of borehole heat exchangers in different aquifers: A case study from Shouguang. *International Journal of Low Carbon Technologies*, doi:10.1093/ijlct/cts043.

Waples, D.W., Waples, J.S. (2004a). A review and evaluation of specific heat capacities of rocks, minerals, and subsurface fluids. Part 1: Minerals and Nonporous rocks. *Natural Resources Research* 13(2), 97–122.

Waples, D.W., Waples, J.S. (2004b). A review and evaluation of specific heat capacities of rocks, minerals, and subsurface fluids. Part 2: Fluids and porous rocks. *Natural Resources Research* 13(2), 123–130.

Ward, J.D., Simmons, C.T., Dillon, P.J. (2007). A theoretical analysis of mixed convection in aquifer storage and recovery: How important are density effects? *Journal of Hydrology* 343, 169–186.

Webmineral. (2011). Webmineral: Basic information for minerals. Accessed on May, 15, 2011, at http://webmineral.com.

Whitaker, S. (1977). Simultaneous heat, mass and momentum transfer in porous media: A theory of drying. *Advances in Heat Transfer* 13, 119–203.

Williams, P.J., Smith, M.W. (1989). *The Frozen Earth. Fundamentals of Geocryology*. Cambridge University Press, Cambridge, UK.

Woodbury, A.D., Smith, L. (1985). On the thermal effects of three-dimensional groundwater flow. *Journal of Geophysical Research* 90(B1), 759–767.

Woodside, W., Messmer, J.H. (1961). Thermal conductivity of porous media. 1. Unconsolidated sands. *Journal of Applied Physics* 32(9), 1688–1698.

Woumeni, R.S., Vauclin, M. (2006). A field study of the coupled effects of aquifer stratification, fluid density, and groundwater fluctuations on dispersion assessments. *Advances in Water Resources* 29, 1037–1055.

Yang, W., Shi, M., Liu, G., Chen, Z. (2009). A two-region simulation model of vertical U-tube ground heat exchanger and its experimental verification. *Applied Energy* 86, 2005–2012.

Xu, M., Eckstein, Y. (1995). Use of weighted least-squares method in evaluating of the relationship between dispersivity and field scale. *Ground Water* 33(6), 905–908.

Zarrella, A., Scarpa, M., De Carli, M. (2011). Short time step analysis of vertical ground-coupled heat exchangers: The approach of CaRM. *Renewable Energy* 36, 2357–2367.

Zeng, H., Diao, N., Fang, Z. (2003). Heat transfer analysis of boreholes in vertical ground heat exchangers. *International Journal of Heat and Mass Transfer* 46, 4467–4481.

Zhu, K., Blum, P., Ferguson, G., Balke, K.-D., Bayer, P. (2010). Geothermal potential of urban heat islands. *Environmental Research Letters* 5, 044002, doi:10.1088/1748-9326/5/4/044002.